Elsevier Editorial System(tm) for Lithos
Manuscript Draft

Manuscript Number:

Title: Petrological and noble-gas features of Lascar and Lastarria volcanoes (Chile): inferences on plumbing systems and mantle characteristics

Article Type: Regular Article

Keywords: Lascar; Lastarria; Noble Gases; Fluid inclusions; Mantle

Corresponding Author: Dr. Philippe Robidoux, Ph.D.

Corresponding Author's Institution: University of Palermo, Dipartimento di Scienze della Terra e del Mare; INGV-Palermo

First Author: Philippe Robidoux, Ph.D.

Order of Authors: Philippe Robidoux, Ph.D.; Andrea Luca Rizzo; Felipe Aguilera; Alessandro Aiuppa; Mariano Artale; Marco Liuzzo; Manuela Nazzari; Filippo Zummo

Abstract: Lascar (5,592 m a.s.l.) and Lastarria (5,697 m a.s.l.) are Chilean stratovolcanoes located in the Central Volcanic Zone (16°S to 28°S) that have developed over-71 km of continental crust. Independently of the similarities in their Plinian/Vulcanian eruptive styles, their complex magmatic feeding structures and the origins of their magmatic fluids still necessitate constraints in order to improve the reliability of geochemical monitoring. Here we investigate the petrography, bulk-rock chemistry, and mineral chemistry in products from the 1989-1993 explosive eruptive cycle at Lascar and from several Holocene eruptive sequences at Lastarria. These data are integrated with measurements of the noble-gas isotopes in fluid inclusions of minerals from the same products as well as in fumarole gases. Petrography, bulk-rock chemistry, and mineral chemistry show that the studied rocks belong to high-K-calc-alkaline series and provide evidence of differentiation, mixing, and crustal assimilation. The deepest crystallization processes occurred at variable levels of the plumbing systems according to the lithostatic equivalent depths estimated with mineral equilibrium geobarometers at Lascar (15-29 km) and Lastarria (~20-40 km). The 40Ar/36Ar and 4He/20Ne ratios indicate the presence of some degree of air contamination in the fluids from both volcanoes. The 3He/4He values at Lascar (6.91-7.12 Ra) are relatively homogeneous and comparable to those of fumaroles, suggesting a main zone of magma crystallization and degassing. In contrast, the 3He/4He values at Lastarria (5.31-8.01 Ra) vary over a wide range, suggesting various magma storage levels and providing evidence of crustal contamination, as indicated by the rock chemistry. We argue that mantle beneath the two volcanoes could have slight differences induced by distinct subducting rocks and conditions. However, we cannot exclude that crustal contamination contributes to the different measured signatures.

Research Data Related to this Submission

There are no linked research data sets for this submission. The following reason is given:
Data will be made available on request

Cover letter

Dr X-H Li
Editor in-chef
Lithos

Santiago, December 24 2019

Dear Dr Li,
Please find here, our manuscript: "Petrological and noble-gas features of Lascar and Lastarria volcanoes (Chile): inferences on plumbing systems and mantle characteristics ", authors: Robidoux, P., Rizzo, A.L., Aguilera F., Aiuppa A., Artale M., Liuzzo M., Nazzari M., Zummo F.", which we submit for your consideration as an article for Lithos.

We report here on the first direct measurements of noble gas (He-Ne-Ar) isotopic compositions in fluid inclusions in olivine and pyroxene crystals at Lascar and Lastarria volcano, Chile. The magmas produced by both stratovolcanoes, since Holocene, represent MORB-like and volcanic arc signatures contaminated by crust according to bulk rock chemistry. Most important, during the last decades, Lascar still hold noble gas values coinciding with fluids trapped in fluid inclusions from mafic minerals sampled in eruptive material from the 1989-1993's period of activity. In comparison, Lastarria volcano show primitive MORB values in Holocene products, but large heterogeneities on dataset rather may represent cortical and atmospheric contamination on ascending magma through a complex plumbing system with different ponding zones below the Andean Cordillera.

Our results contribute to a better understanding of the mantle fluid chemistry from magmas that travel in plumbing system form typical active stratovolcanoes in Northern Chile, and allow refining a novel petrological method to discriminate fluid sources from fumaroles at monitored volcanoes.

For the reasons above, we believe our study would attract the attention of a variety of earth scientists interested by petrological processes in active volcanoes, from matnle-to-lithospheric conditions. Given the inherent practical contribution of the investigation for volcanic risks and applied petrology, we believe that Lithos would make a perfect output for our manuscript.

I shall act as the corresponding author for this article, and I may be contacted using the details found below. I can confirm that this work is original, and is neither published, nor under consideration for publication elsewhere.

The following four individuals would be well qualified to act as reviewers for this manuscript:

1. Qiang Wang, Guangzhou Institute of Geochemistry State Key Laboratory of Isotope Geochemistry, Guangzhou, China
2. Andrew C. Kerr Editorial Board, Lithos Cardiff University School of Earth and Ocean Sciences, Cardiff, United Kingdom
3. Dan Harlov, Helmholtz Centre Potsdam German Research Centre for Geosciences, Potsdam, Germany
4. Gray Bebout, Lehigh University, Bethlehem, Pennsylvania, United States

Yours Sincerely
Philippe Robidoux

Via Ersilia 803, Santiago, Chile – Tel. +56951232150 –
e-mail: robidouxphilippe@gmail.com

Abstract: Lascar (5,592 m a.s.l.) and Lastarria (5,697 m a.s.l.) are Chilean stratovolcanoes located in the Central Volcanic Zone (16°S to 28°S) that have developed over–71 km of continental crust. Independently of the similarities in their Plinian/Vulcanian eruptive styles, their complex magmatic feeding structures and the origins of their magmatic fluids still necessitate constraints in order to improve the reliability of geochemical monitoring. Here we investigate the petrography, bulk-rock chemistry, and mineral chemistry in products from the 1989–1993 explosive eruptive cycle at Lascar and from several Holocene eruptive sequences at Lastarria. These data are integrated with measurements of the noble-gas isotopes in fluid inclusions of minerals from the same products as well as in fumarole gases. Petrography, bulk-rock chemistry, and mineral chemistry show that the studied rocks belong to high-K–calc-alkaline series and provide evidence of differentiation, mixing, and crustal assimilation. The deepest crystallization processes occurred at variable levels of the plumbing systems according to the lithostatic equivalent depths estimated with mineral equilibrium geobarometers at Lascar (15–29 km) and Lastarria (~20–40 km). The $^{40}Ar/^{36}Ar$ and $^{4}He/^{20}Ne$ ratios indicate the presence of some degree of air contamination in the fluids from both volcanoes. The $^{3}He/^{4}He$ values at Lascar (6.91–7.12 Ra) are relatively homogeneous and comparable to those of fumaroles, suggesting a main zone of magma crystallization and degassing. In contrast, the $^{3}He/^{4}He$ values at Lastarria (5.31–8.01 Ra) vary over a wide range, suggesting various magma storage levels and providing evidence of crustal contamination, as indicated by the rock chemistry. We argue that mantle beneath the two

volcanoes could have slight differences induced by distinct subducting rocks and conditions. However, we cannot exclude that crustal contamination contributes to the different measured signatures.

Highlights

- Lascar noble gases in fumaroles coincident with trapped fluids in crystals
- Bulk rock and crystal chemistry at Lastarria reflect larger magma residence times
- Deepest polybaric crystal fractioning conditions at Lascar and Lastarria at 40 km
- Subducting magmas with MORB and volcanic arc signatures contaminated by crust

Petrological and noble-gas features of Lascar and Lastarria volcanoes (Chile): inferences on plumbing systems and mantle characteristics

*Robidoux P.[1], Rizzo A.L.[2], Aguilera F.[3], Aiuppa A.[4], Artale M.[4], Liuzzo M.[2], Nazzari M.[5], Zummo F.[4]

[1]Centro de Excelencia en Geotermia de Los Andes CEGA, Universidad de Chile, Santiago, Chile

[2]Istituto Nazionale Di Geofisica e Vulcanologia, Sezione Palermo, Palermo, Italy

[3]Universidad Católica del Norte, Antofagasta, Chile

[4]Dipartimento DiSTeM, Università di Palermo, Palermo, Italy

[5]Istituto Nazionale Di Geofisica e Vulcanologia, Sezione Roma, Rome, Italy

*Corresponding author at:

Centro de Excelencia en Geotermia de Los Andes CEGA

Departamento de Geología

Facultad de Ciencias Físicas y Matemáticas

Universidad de Chile, Santiago, Chile

Tel.: +56 951232150

E-mail: robidouxphilippe@gmail.com

Keywords: Lascar, Lastarria, Noble gases, Fluid inclusions, Mantle

Abstract: Lascar (5,592 m a.s.l.) and Lastarria (5,697 m a.s.l.) are Chilean stratovolcanoes located in the Central Volcanic Zone (16°S to 28°S) that have developed over–71 km of continental crust. Independently of the similarities in their Plinian/Vulcanian eruptive styles, their complex magmatic feeding structures and the origins of their magmatic fluids still necessitate constraints in order to improve the reliability of geochemical monitoring. Here we investigate the petrography, bulk-rock chemistry, and mineral chemistry in products from the 1989–1993 explosive eruptive cycle at Lascar and from several Holocene eruptive sequences at Lastarria. These data are integrated with measurements of the noble-gas isotopes in fluid inclusions of minerals from the same products as well as in fumarole gases. Petrography, bulk-rock chemistry, and mineral chemistry show that the studied rocks belong to high-K–calc-alkaline series and provide evidence of differentiation, mixing, and crustal assimilation. The deepest crystallization processes occurred at variable levels of the plumbing systems according to the lithostatic equivalent depths estimated with mineral equilibrium geobarometers at Lascar (15–29 km) and Lastarria (~20–40 km). The $^{40}Ar/^{36}Ar$ and $^{4}He/^{20}Ne$ ratios indicate the presence of some degree of air contamination in the fluids from both volcanoes. The $^{3}He/^{4}He$ values at Lascar (6.91–7.12 Ra) are relatively homogeneous and comparable to those of fumaroles, suggesting a main zone of magma crystallization and degassing. In contrast, the $^{3}He/^{4}He$ values at Lastarria (5.31–8.01 Ra) vary over a wide range, suggesting various magma storage levels and providing evidence of crustal contamination, as indicated by the rock chemistry. We argue that mantle beneath the two

volcanoes could have slight differences induced by distinct subducting rocks and conditions. However, we cannot exclude that crustal contamination contributes to the different measured signatures.

1. Introduction

Lascar and Lastarria (Chile) are two of the most actively degassing quiescent stratovolcanoes in the Central Volcanic Zone (CVZ) (Tamburello et al., 2015), and they have a long record of volcanic eruptions with magnitudes up to Plinian/Vulcanian. Lascar erupted frequently during the Holocene, and a recent short-lived magmatic intrusive event was responsible for major explosive eruptions in 1993 (Matthews et al., 1994; Gardeweg et al., 1998, 2011; Calder et al., 2000). Lastarria has exhibited major explosive eruptions separated by longer time intervals compared with those at Lascar (Aguilera, 2008; Naranjo, 2010).

The available petrological and geophysical information indicates that the two volcanoes have complex plumbing systems and different magma residence times in crustal reservoirs (Naranjo, 2010; Aguilera et al., 2012). For example, the 1993 eruptive products are thought to have erupted from the superficial (~2 km deep) magma ponding zone at Lascar, although mineral–melt equilibria imply a vertically elongated plumbing system extending as deep as 11.5 km (up to ~500 MPa; Stechern et al., 2017). Seismic tomography has indicated that magma could actually be stored from as shallow as ~1 km to as deep as 5–6 km at Lastarria (Spica et al., 2015).

Despite numerous studies, the complex magmatic feeding systems and the origin of magmatic volatiles remain only partially understood at both volcanoes. In addition, despite the volcanoes being located at the edge of the Andean subduction zone above ~71 km of rigid continental crust (Thorpe et al., 1982), the impact of crustal assimilation on the composition of intruding magma is poorly understood. It remains unclear whether the magmatic fluids that today feed fumarole emissions originate from fresh and undegassed newly ascending magma or from more-aged stored melts.

In this work we combine petrological data with noble-gas analyses of fluid inclusions (FIs) in olivines and clinopyroxenes (Cpx) to address some of the above open questions. We report on the major-element chemistry of the mineral assemblage integrated with analyses of bulk-rock major and trace elements to characterize the mantle contribution of magma and levels of magma storage below Lascar and Lastarria volcanoes. We also attempt to identify possible differences between the two plumbing systems, and the role of continental crust in contaminating magma compositions. FI noble-gas isotope signatures are compared with new information and that in the literature on the fumaroles to assess shallow atmospheric contamination, and mantle versus crustal origins of volatiles in the shallow plumbing systems.

2. Geological and geodynamic setting

Orogenic andesitic stratovolcanoes from the Neogene to the present day along the South American Volcanic Arc are structurally and compositionally grouped in three main zones from north to south: (1) Northern Volcanic Zone (5°N to 2°S), (2) CVZ (16°S to 28°S), and (3) Southern Volcanic Zone (33°S to 52°S) (Thorpe and Francis, 1979; Thorpe et al., 1982; Harmon et al., 1984). From north to south the crust thickness varies between 30 and 71 km. The variable depth of the Benioff plan (80–120 km) plays a major role in delivering slab fluid and the partial melting of the mantle wedge, while crustal assimilation impacts the K content of the magma (Stern, 2004), contributing to defining calc-alkaline (CA) versus shoshonitic volcanic rock series (Stern, 2004). The convergence rate averages 7 cm/year (DeMets et al., 2010) and trench structures vary from deep, dry, and sediment-poor in the north, to shallow and sediment-rich in the south (Völker et al., 2013).

2.1 Chemistry of CVZ magmas

Magmas in the Andean CVZ are mainly andesites to dacites, but some mafic and felsic endmember magmas have also been found (Wörner et al., 2018 and references therein). The continental crust contamination is greater in CVZ magmas than in the rest of the South American Volcanic Arc, as testified by their higher $^{87}Sr/^{86}Sr$, $^{207}Pb/^{204}Pb$, and $^{208}Pb/^{204}Pb$ ratios, and lower $^{143}Nd/^{144}Nd$ ratios (e.g. Harmon et al., 1984; Thorpe et al., 1984; Hickey et al., 1986; Hildreth and Moorbath, 1988; de Silva, 1991; Davidson and de Silva, 1992; Wörner et al., 1994; Haschke et al., 2006; Mamani et al., 2008, 2010; Jacques et al., 2014; Kay et al., 2014; Scott et al., 2018; Wörner et al., 2018). Overall the Sr and Pb isotope concentrations decrease (and the Nd concentrations increase) with the age of rocks, except for the majority of the Mesozoic volcanic fields and ignimbrites that include evolved endmembers (de Silva et al., 2006).

The patterns of rare earth elements (REE) are typical of volcanic arc settings, but indicate frequent heterogeneities with N-MORB, E-MORB, and OIB signatures due to large variations in different accreted terrains (Mamani et al., 2008, 2010 and references therein).

2.1.1 Lascar volcano

Lascar volcano (23.37°S and 67.73°W, 5,592 m a.s.l.) is a stratovolcano located in the central part of the CVZ (Fig. 1). This volcano comprises two cones hosting five nested craters trending along an ENE–WSW direction. The central crater is the currently active vent and is characterized by intense fumarole activity. Records of eruptive activity date back to the 19th century and cover more than 40 eruptions (e.g., Aguilera, 2004 and references therein). The activity was most intense between 1984 and 1994, when three main dome growth-and-collapse cycles generated lava domes that were successively destroyed by moderate Vulcanian eruptions (Matthews et al., 1997).

The most-prominent event recorded in historical time was the 1993 sub-Plinian eruptive phase. The eruption emitted 0.1 km^3 of rocks, generating eruptive columns that reached up to 25 km, pyroclastic flows going down the NW and SE flanks extending as far as 8 km from the active crater (Gardeweg and Medina, 1994), and falls of tephra that were detected in Argentina, Paraguay, Brazil, and Uruguay (BGVN, 1994). The last explosion was recorded on October

30, 2015, whose eruptive column reached 2.5 km above the active crater (BGVN, 2016). A permanent gas plume is emitted from the active crater, where highly variable SO_2 fluxes have been recorded during 1989–2011, ranging between 150 and 2,300 tons/day (e.g., Andres et al., 1998; Menard et al., 2014).

According to Gardeweg et al. (1998, 2011), Lascar volcano is built over a basement constituted by volcanic/volcaniclastic/sedimentary basements and granitoids rocks from Permian to Miocene. Upper Miocene to Pleistocene strata of large ignimbrite, domes, and volcanic rocks follow the sequence. Gardeweg et al. (2011) divided the evolution of Lascar volcano over the basement into four stages ranging from ca. 240 ky up to the present day (Gardeweg et al., 1998; Calder et al., 2000).

The eruptive products emitted from Lascar volcano belong to moderate-to-high K-CA series. Their $^{86}Sr/^{87}Sr$ isotope ratios and εNd values suggest a moderate crustal contamination (Matthews et al., 1994). The major- and trace-element chemistry revealed by rock analyses suggests that fractional crystallization and magma mixing are the key petrogenetic processes (Matthews et al., 1994).

2.1.2 Lastarria volcano

Lastarria volcano (also called Lastarria sensu stricto; 25.16°S and 68.50°W, 5,697 m a.s.l.) is a composite stratovolcano located in the southern part of the CVZ (Fig. 1). It forms part of a major volcanic structure called the Lastarria Volcanic Complex (LVC), which also includes the Southern Spur volcano and

Negriales lava field (Naranjo, 2010). Lastarria is a single edifice (~10 km^3) constituted by five nested craters that are aligned along a north–south direction. Four permanent fumarole fields are currently located along the rim of crater 4, inside crater 5, and on its northwestern flank, each covering 0.001–0.04 km^2 and characterized by intense fumarole activity (Fig. 1b; Aguilera, 2008).

Lastarria volcano has undergone ground deformation and been characterized by a long period of earthquakes since at least 1997 (Pritchard and Simons, 2004; Froger et al., 2007). A major deformation is centered on the so-called Lazufre area (constituting the LVC, Cordón del Azufre, and Bayo volcanoes), with a depth of 7–15 km and a deformation rate of 2–3 cm/year, with some areas related to an overpressure source (e.g., boiling aquifer) lying 1,000 m below the crater area (Pritchard and Simons, 2002; Froger et al., 2007; Ruch et al., 2009; Budach et al., 2013; Spica et al., 2015; Díaz et al., 2015).

The LVC has formed over Upper Miocene/Upper Pleistocene volcanic rocks corresponding to andesitic-to-dacitic lava flows and domes, with subordinate basaltic andesite lava flows (Naranjo, 1992, 2010). Pyroclastic rocks corresponding to Lower Pleistocene dacitic ignimbrites are also present.

Naranjo (2010) summarized the geological evolution of the LVC into three major volcanic structures: (1) Negriales lava field (400±60 to 116±26 ky [mean±SD]; Middle to Upper Pleistocene), (2) Espolón Sur (Southern Spur) (150±50 ky; Middle Pleistocene), and (3) Lastarria sensu stricto. Naranjo divided the evolution of the LVC into 10 stages ranging from 330±100 to 249±36 ky (Middle Pleistocene) up to the Holocene and present day.

The eruptive products from Lastarria volcano belong to high-K calc-alkaline (HK-CA) series (Mamani et al., 2008, 2010; Naranjo, 2010). The compositions of Sr, Nd, and Pb isotopes (Trumbull et al., 1999; Mamani et al., 2008, 2010) suggest high levels of crustal contamination due to a thick continental crust (Trumbull et al., 1999).

3. Sampling and methods

3.1 Sampling locations

3.1.1 Rocks

The Lascar rock samples LAS1, LAS2, and LAS3 are crystal-rich scoriae from pyroclastic-flow deposits emitted from the central crater (Table 1). The youngest material collected was emitted during the sub-Plinian eruption in April 18–21, 1993 (Gardeweg et al., 1993; Matthews et al., 1994; Sparks et al., 1997; Calder et al., 2000). Distant pyroclastic deposits located on the northwestern flank were found to be abundant in white pumices (Matthews et al., 1994) and dark-color clasts of large scoria bombs and crystalline blocks (up to 1 m). The white and vesicular pumices (described and studied by Matthews et al., 1994; Sparks et al., 1997; Calder et al., 2000) were not collected because they are not associated with the mafic juvenile source and do not contain large quantities of visible olivines and pyroxenes. Our sampling thus preferentially targeted the dark scoria with sizes ranging from lapilli to bombs and gray block fragments of the pyroclastic-flow deposits. More specifically, we present data for the crystalline porphyric dome fragments emitted during 1989-1990 (LAS1) and juvenile scoria (LAS2) (Matthews et al., 1994).

We also studied the Tumbres scoriaceous pyroclastic flow (ca. 9.2 ky; Gardeweg et al., 2011) sampled in outcrops in the southern Tumbres area and in the Talabre Viejo canyon. This sampling site corresponds to the northeastern border of the flow, and several fragments weighing >3 kg were taken from large scoria bombs (LAS3). Textures were similar to LAS2 scoriae, but the LAS3 scoriae presented alternating gray and beige surfaces. Full details on the locations of the deposits are presented in Table 1.

Sampling at Lastarria was performed on the northwestern flank and concentrated on Holocene pyroclastic-flow deposits containing scoriaceous lapilli and bombs, banded black and beige pumices, and lithic block components (Table 1; Naranjo, 2010). LRA1 and LRA2 are scoria fragments with sizes ranging from lapilli to bombs that fall under the “grey IV pyroclastic flow deposit” definition reported by Naranjo (1992), later renamed as “Ignimbrite 3” by Naranjo (2010) (Table 1 provides a list of equivalent names). This flow was emitted by crater 4, where most of the actual summit fumaroles are located (Aguilera, 2008). The pyroclastic deposit is dated 2.46±0.04 ky A.P. (Naranjo, 2010). The LRA3 sample consists of crystalline pumice fragments from the ~2.5–4.8 ky (~late Holocene) Ignimbrite 2 of Naranjo (2010), corresponding to the “grey I pyroclastic flow deposit” defined by Naranjo (1985, 1992). The LRA4 rock samples are pale crystalline pumice fragments emitted by crater 3, which is older. From the position of the sampling site, petrographic features, and stratigraphic position (the fragments are white pumices covering the superior layer of the flow margin), we infer that LRA4 is associated with the 4.85±0.04 ky A.P. Ignimbrite 1 described in Naranjo (2010), and more specifically with the “pink pyroclastic flow deposit” defined by Naranjo (1992).

3.1.2 Gases

Fumarole gas samples were collected on the northwestern flank of Lastarria during the 2014 IAVCEI CCVG (Commission on Chemistry of Volcanic Gases) 12th Volcanic Gas Workshop (Lopez et al., 2018). Gas was sampled using a titanium tube inserted into the fumarole soil, then connected to a quartz line, with a silicone tube equipped with a three-way valve connected to a syringe for pumping the gas. Dry gases were finally stored in glass bottles for subsequent laboratory analyses. Further details of the study protocol can be found in Lopez et al. (2018).

3.2 Analytical techniques

3.2.1 Bulk-rock major and trace elements

Rock samples were prepared for analyzing major and trace elements in the DiSTeM laboratory at the University of Palermo. Bulk-rock analyses were performed at Activation Laboratories (Ancaster, Canada) following techniques described in i.e. Di Piazza et al. (2015) and Robidoux et al. (2017).

3.2.2 Mineral and glass chemistry

The mineral chemistry of the FI-hosted minerals was studied using electron microprobe analysis (EMPA). For this purpose, sampled blocks, scoria, and pumice fragments containing phenocrysts (Tables 1 and 2) were crushed and sieved several times until a homogeneous grain size of 0.5–1.0 mm was obtained. Several number of phenocrysts in this granulometric size range at Lascar (n=163) and Lastarria (n=138) were then characterized. Dense phenocrysts (>2.63 g/cm^3) were separated from scoria, and less-dense minerals (e.g., plagioclase) were separated using sodium polytungstate liquid columns. The separated minerals were collected and washed with deionized water and acetone. The remaining scoria and plagioclase samples were also stored and washed.

Mineral chemistry was analyzed at the HPHT (high-pressure/high-temperature) laboratory of Istituto Nazionale di Geofisica e Vulcanologia (INGV) in Rome using an electron microprobe analyzer (JXA-8200, JEOL) equipped with five wavelength-dispersive X-ray spectrometers and one energy-dispersive X-ray spectrometer analyzer. Plagioclases, olivines, Cpx/orthopyroxenes (Opx), and biotites were all prepared on different mounts after using abrasives and polishing down to 6-, 3-, and 1-µm diamond powder fractions. A set of reference crystals was used for quantifying major elements (the measurement uncertainties are described in Appendix I). At least two spots on both the core and rim of each crystal were analyzed to identify composition changes during crystal growth (Appendixes I–V).

Matrix glass on the rim of separated phenocrysts and background (matrix) glass obtained from prepared thin sections were probed by EMPA. Glass surfaces from phenocrysts and closed inclusions with glassy texture were selected to study the chemical equilibrium in liquid–mineral and Opx–Cpx associations. The EMPA conditions were a beam current of 7.50 nA, accelerating voltage of 15 kV, and beam diameter of 5 µm. The counting times for the minerals were 10 and 5 s at the peak and background, respectively.

3.2.3 Noble-gas element and isotope compositions

3.2.3.1 Fumaroles

The concentrations and isotope compositions of noble gases (He and Ne) in fumarole gases were determined at the INGV laboratories in Palermo. The ^{3}He, ^{4}He, and ^{20}Ne concentrations were measured separately in a split-flight-tube mass spectrometer (GVI-Helix SFT, for analyzing the He isotopes) and in a multicollector mass spectrometer (Thermo-Helix MC Plus, for analyzing ^{20}Ne) after applying standard purification procedures (Di Piazza et al., 2015; Rizzo et al., 2015, 2016). The $^{3}He/^{4}He$ ratio was expressed in units of R/Ra (where Ra is the He-isotope ratio of air, 1.39×10^{-6}), and the analytical uncertainty (1σ) in single measurements was generally <0.3% (Table 3). The used standard was air, whose reproducibility across >50 analyses performed over several months was <3%. The $^{3}He/^{4}He$ ratios were corrected for atmospheric contamination using the measured $^{4}He/^{20}Ne$ ratio (e.g., Sano and Wakita, 1985; Rizzo et al., 2015) as follows:

$$R/Ra=((RM/Ra)(He/Ne)_M - (He/Ne)_A)/((He/Ne)_M - (He/Ne)_A) \quad (1)$$

where subscripts M and A refer to measured and atmospheric values, respectively [$(He/Ne)_A$=0.318]. The corrected $^3He/^4He$ ratios are reported in the main text and Table 3 as Rc/Ra values. The correction is small or negligible for most of the samples, with the maximum bias of ~0.2 Ra appearing in the sample showing the lowest $^4He/^{20}Ne$ value.

The Ar concentrations and isotope compositions (^{36}Ar, ^{38}Ar, and ^{40}Ar) were quantified in a multicollector mass spectrometer (Helix MC-GVI). The analytical uncertainty (1σ) for single $^{40}Ar/^{36}Ar$ measurements was <0.1%. The used standard was air, whose reproducibility over 1 year of daily analyses was <3.5%.

Typical blanks for He, Ne, and Ar were $<10^{-15}$, $<10^{-16}$, and $<10^{-14}$ mol, respectively, and are at least two orders of magnitude lower than the sample signals.

3.2.3.1 FIs in olivine and pyroxene crystals

The element and isotope compositions of He, Ne, and Ar were measured in FIs hosted in the olivine and pyroxene crystals at the INGV laboratories in Palermo (Table 4). Fluids are trapped as spherical or ellipsoidal gas or liquid bubbles during and after magma crystallization (Roedder, 1979, 1984). The olivine and pyroxene crystals were separated from fractions with sizes of 0.5–1 mm. The selected crystals were then cleaned and prepared for noble-gas measurements in accordance with a reproductible protocol (i.e. consult Di Piazza et al., 2015; Rizzo et al., 2015; Robidoux et al., 2017; Battaglia et al., 2018). Each group of samples (0.1–1.3 g) was then loaded into a six-position stainless-steel crusher. Noble gases trapped inside the FIs were released after in-vacuo single-step crushing, which minimizes the contribution of cosmogenic ^{3}He and radiogenic ^{4}He that could be trapped in the crystal lattice (e.g., Hilton et al., 2002; Rizzo et al., 2015).

He isotopes (^{3}He and ^{4}He) and ^{20}Ne were measured separately by two different split-flight-tube mass spectrometers (Helix SFT-Thermo). The analytical uncertainty (1σ) of the He-isotope ratio measurements was <5%. The used standard was air, whose reproducibility across >20 analyses performed over several months was <2%.

Ar isotopes (^{36}Ar, ^{38}Ar, and ^{40}Ar) were analyzed by a multicollector mass spectrometer (GVI Argus) at an analytical uncertainty (1σ) of <0.4%. The used standard was air, whose reproducibility across analyses performed over >2 years was <1%.

Typical blanks for He, Ne, and Ar were $<10^{-14}$, $<10^{-16}$ and $<10^{-14}$ mol, respectively, and were at least one order of magnitude lower than the values measured in the samples. Further details about the sample preparation and analytical procedures are available in Di Piazza et al. (2015), Rizzo et al. (2015), Robidoux et al. (2017), and Battaglia et al. (2018).

4 Results

4.1 Bulk-rock geochemistry

4.1.1 Lascar volcano

The major-element compositions of bulk-rock samples are presented in Table 2. Our Lascar rock samples are andesitic (Fig. 2a) and fairly homogeneous (SiO_2=58.1–58.3 wt%, K_2O=1.56–1.62 wt%), and thus overlap with the compositions of the least-differentiated Lascar mafic enclaves and 1993 eruption products (e.g., Matthews et al., 1994, 1999). The bulk-rock composition range for Lascar is wider in the published literature, ranging from andesitic to dacitic (SiO_2<56.6–69.4 wt%, K_2O=1.3–3.8 wt%) and falling within the fields of CA and HK-CA series (Deruelle, 1982; Matthews et al., 1994, 1999; Mamani et al., 2010) (Fig. 2a).

Lascar trace-element rock compositions exhibit smaller light rare earth elements (LREE) enrichments when “N” is normalized to the C1 chondrite values from McDonough (1995) (La/Yb_N=11.2–13.2). The Eu anomaly is small and constant (Eu/Eu*=0.80–0.86). Lascar rocks are slightly enriched in large-ion lithophile elements (e.g., Cs, Rb, and Ba) relative to N-MORB, and they overlap with E-MORB. Most samples have low contents of the high-field-strength elements (HFSE) Ta, Nb, Zr, and Hf. The Lascar rocks exhibit moderate Ba/La_N and U/Th_N values, ranging from 35.9–41.4 and 0.24–0.28, respectively (Table 2).

4.1.2 Lastarria volcano

Figure 2b plots the bulk-rock compositions of our Lastarria samples in the context of the results obtained in previously reported studies. Our samples are intermediate to felsic (SiO_2=58.2–63.4 wt%, K_2O=2.0–3.1 wt%) (Table 2), and fall within the same HK-CA series evolutionary trend (Mamani et al., 2010) defined by bulk-rock literature data (SiO_2=58.6–69.4 wt%, K_2O=2.0–3.8 wt%; Naranjo, 1992; Stechern et al., 2017) (Fig. 2b). Our LRA3 and LRA2 samples are among the least-differentiated Lastarria rocks (Naranjo, 1992), while sample LRA4 (taken from Ignimbrite 1 emitted by crater 3) is more evolved (SiO_2=63.4 wt%). Our sample LRA4, although evolved, has a lower silica content than the most-differentiated Lastarria group of samples: the Negriales lava field (Naranjo, 1992; Fig. 2b). Overall, our rock samples (LRA2, LRA3, and LRA4) are alkali-rich (>5.3 wt%) and have low Mg# values (<53.0%).

Trace elements in Lastarria rocks show moderate LREE enrichments (La/Yb_N=25.4–30.1), small Eu anomalies (Eu/Eu*=0.73–0.82), and are richer in large-ion lithophile elements (e.g., Cs, Rb, and Ba) compared with Lascar. Most samples have low contents of HFSE, but the concentrations are slightly higher than those at Lascar (Table 2). The Lascar rocks exhibit moderate Ba/La_N and U/Th_N values (27.9–32.0) and low U/Th_N values (0.23–0.24) (Table 2).

4.2 Petrography and mineral chemistry

4.2.1 Lascar volcano

The phenocryst concentration decreases in the following order at Lascar: plagioclase > Cpx > Opx > olivine > magnetite. Dome fragments (LAS1) are nonvesicular and densely microporphyric. Scoriae fragments (LAS1 and LAS2) with sizes from lapilli to bomb are all porphyric, but they exhibit various degrees of vesicularity. The LAS1 xenocrystals represent a coarse granulate cumulate of Cpx-plagioclase assemblage found in the dome fragment. The major-element concentrations from those cumulates are compared with the rest of the Cpx and plagioclase found as dispersed porphyric mineral phases in Figs. 3 and 4. The full results obtained in the mineral chemistry analyses of Lascar and Lastarria samples are reported in Appendixes II–V and illustrated in Fig. 3.

The LAS1 dome fragments mainly contain porphyric plagioclases ($An_{46–60}$) and green Cpx here identified as augite species ($Wo_{38–50}En_{39–46}Fs_{8–14}$) with moderate Mg# values (Mg/(Mg+Fe)=71–86%, average 81%; Fig. 3c). Cpx of 1993 materials (LAS1) are closer to the diopside endmember than to augite (e.g., Linsley, 1983). Three of seven core–rim Cpx pairs show normal zoning, but the rest have homogeneous compositions, while four of five core–rim pairs for LAS1 crystals show normal zoning (Fig. 3c). Three of six samples of LAS2 augite phenocrysts have normal zoning, while five LAS3 core–rim pairs have reverse zoning, five have normal zoning, and one is homogeneous. The greenish Cpx found in LAS3 (augite; $Wo_{41–52}En_{40–46}Fs_{6–15}$) have moderate Mg# values (81±5%) and compositions similar to that of LAS2 (Fig. 3c). Matthews (1994) reported that 1993 scoria and pumice exhibit lower Mg# values of 73–78% and 73–82%, respectively.

In the dark scoria of the 1993 eruption (LAS1), pyroxenes-plagioclase granular cumulates are found with similar compositions to phenocrysts of augite sampled in the rest of the rock fragments ($Wo_{40–53}En_{39–46}Fs_{5–17}$ with Mg#=71–87% and 80±5%) and plagioclase ($An_{46–70}$). One distinction is that the plagioclases in cumulates are rather heterogeneous and richer in Na, with few crystals reaching consistency with the andesine group (Fig. 3f, Appendix IV).

The LAS2 scoria fragments have $An_{43–47}$ plagioclases and abundant green Cpx (augite; $Wo_{39–50}En_{40–45}Fs_{6–16}$) with moderate Mg# values (72–90%, 78±6%). In comparison, the LAS3 older scoria fragments contain labradorites ($An_{47–58}$).

Opx minerals are less abundant (Fig. 3a), with hypersthenes as the dominant species. Sample LAS1 from dome fragments contains hypersthenes ($Wo_{2–4}En_{68–70}Fs_{20–29}$) with moderate Mg# values (71–77%, 75±3%). A particularly interesting finding is that the hypersthene core–rim pairs have Mg# values similar to those of the 1986–1990 Lascar dome samples (69–77%) reported by Matthews (1994). The hypersthenes from LAS2 scoriae show wide Mg# ranges (64–82%). LAS3 scoria hypersthenes have similar compositions ($Wo_{2–3}En_{64–83}Fs_{13–33}$) with moderate Mg# values (66–86%, 75±6%) and thus are similar to the crystals of 1993 scoriae. The Mg# values increase moderately from the core to the rim (Fig. 3a).

The olivines in dome samples were abundant and primitive ($Fo_{76–90}$, $Fo_{83±4\%}$; Fig. 3e). Olivines were not analyzed in the LAS2 scoria and can only be observed under a microscope. The olivines in older scoria (LAS3) are abundant and slightly less primitive ($Fo_{76–86}$, $Fo_{80±4\%}$; Fig. 3e). Only 1 of 18 olivines show reverse zoning, while the rest show forsterite contents decreasing from the core to the rim (Fig. 3e).

4.2.2 Lastarria volcano

Scoriae and pumice blocks have distinct phenocryst assemblages at Lastarria, with a porphyritic texture and a wide range of microphenocryst (void-free) concentrations in the LRA2, LRA3, and LRA4 samples. The phenocryst concentration decreases in the following order: plagioclase > Cpx > Opx > biotite > hornblende (trace) > magnetite. Very few olivine crystals were observed as phenocrysts. Scoriae fragments with sizes ranging from lapilli to bombs are highly vesicular (small pores), and the groundmass is generally microcrystalline to glassy. Pumices have various colors and show signs of mingling, with frequent interconnections between clear and dark bands (e.g., Naranjo, 1992; Stechern et al., 2017).

The mineral assemblage indicates differentiated magmas at Lastarria (forsterite-olivine, Fo_{82}; augite, $Wo_{41–48}En_{38–44}Fs_{9–14}$; hypersthene, $Wo_{1–3}En_{62–70}Fs_{23–35}$; plagioclase, $An_{38–52}$). Substantial compositional dissimilarities exist between different LRA1, LRA2, LRA3, and LRA4 samples (Fig. 3d). Amphiboles and apatites are found also as phenocrysts with spinel/magnetite inclusions and intergrowth (see Stechern et al., 2017).

The LRA2 scoria blocks contain high concentrations of porphyric plagioclases ($An_{22–26}$), while plagioclases in pumice fragments from LRA4 appear more evolved ($An_{37–52}$). Few plagioclases were analyzed overall (n=5). Stechern et al. (2017) classified plagioclases as labradorite and andesine, similarly to the present study (Fig. 3f, Appendix IV).

Scoria LRA2 samples contain Cpx identified as augite species ($Wo_{42–46}En_{39–44}Fs_{11–15}$) with moderate Mg# values (73–81%, 77±2%; Fig. 3d). The augites are slightly more primitive in LRA3 pumices ($Wo_{41–48}En_{40–45}Fs_{9–15}$ with Mg#=74–83%) than LRA4 ($Wo_{42–45}En_{42–44}Fs_{12–15}$ with Mg#=74–78%). For core–rim pairs in LRA2, three of nine phenocrysts exhibit reverse zoning while the rest are homogeneous. In LRA3, 10 core–rim pairs comprise 3 with reverse zoning, 3 with normal zoning, and 4 that are homogeneous. In LRA4, three of six phenocrysts exhibit reverse zoning while the rest are homogeneous.

In LRA2, Opx were analyzed and identified as hypersthene species ($Wo_{1–3}En_{73–83}Fs_{14–24}$; Mg#=70%). In pumice fragments from LRA3 fragments, hypersthenes are found as intergrowth Cpx-Opx crystals ($Wo_3En_{83}Fs_{14}$), whereas augites are more differentiated ($Wo_{2,3}En_{73–74}Fs_{22–24}$). In LRA4, pumice fragments contain hypersthenes ($Wo_{2,3}En_{67–74}Fs_{25–33}$) with moderate Mg# values (66–73%). Zoning does not appear frequently (being observed in only 6 of 18 samples, mostly in LRA4), among which 2 of 6 crystals show reverse zoning.

Micas are frequent in pumice fragments and include several large glass inclusions, but many contain plagioclase and pyroxene solid inclusions. The Fe contents estimated from stoichiometric calculations (Deer, 1992) indicate that most micas have Fe/(Fe+Mg) ratios of 0.28–0.32 (Appendix V). Those ratios are thus close to the phlogopite–biotite transition (Fe/(Fe+Mg)=0.33). Micas have $Si/Al^{(IV)}$ ratios of 2.40–2.48.

4.3 Glass inclusions and matrix glass compositions

4.3.1 Lascar volcano

Matrix glasses around phenocrysts were probed to verify mineral–liquid equilibrium (Appendix VI). Spherical and ellipsoidal glass inclusions were also observed and analyzed, but the differentiated nature of those inclusions (SiO_2=73.8–76.8 wt%, K_2O=3.5–4.2 wt%; Fig. 2a) made it difficult to use them for barometry calculations (see below). Only hypersthene and augite euhedral crystals have fully enclosed glassy inclusions without postentrapment characteristics, so their major-element compositions are likely to be unaffected by elemental diffusion in crystal hosts (Danyushevsky et al., 2004). The crystal host compositions are listed in Appendix VII.

Lascar matrix glasses are andesitic to trachytic and follow steep K-versus-Si evolution trends (Fig. 2a; SiO_2=61.0–72.1 wt%, K_2O=1.0–5.1 wt%). The most-primitive glasses are found around hypersthene minerals from dome fragments (SiO_2=61.0–70.0 wt%, K_2O=1.0–4.5 wt%, Mg#≤36%), while most Cpx and plagioclase glass rims are trachytic to rhyolitic. Figure 4a demonstrates that magnesium distribution coefficients measured from sets of mineral–glass couples are below olivine ($Kd_{Fe\text{-}Mg}$=0.30±0.03) or Cpx ($Kd_{Fe\text{-}Mg}$=0.27±0.03) equilibrium values, with a few exceptions. The Cpx-plagioclase cumulates contrast the most from the mineral–liquid Kd being in equilibrium (Fig. 4a), and so they were considered as xenocrystals in this study.

4.3.2 Lastarria volcano

Lastarria matrix glasses exhibit andesitic, banakitic, and trachytic compositions (SiO_2=62.3–76.6 wt%) and are particularly rich in K (K_2O=2.3–5.6 wt%). Hypersthene glass rims exceptionally show evolved rhyolitic compositions (SiO_2>75.5 wt%, K_2O>5.0 wt%, Mg#<26.3%), and are richer in alkalis compared with Lascar (Fig. 2b, Appendix VI).

Spherical and ellipsoidal glass inclusions are also rather evolved (SiO_2=53.7–75.9 wt%, K_2O=0.6–6.0 wt%). Opx, Cpx, and biotite crystals have fully enclosed glass inclusions without postentrapment characteristics. The crystal host compositions are listed in Appendix VII, and the mineral host compositions from biotite are listed in Appendix V.

Distribution coefficients for Fe are closer to equilibrium values than for the Lascar samples (Fig. 4). In total, two inclusions and three glasses cross the equilibrium lines within the margin of error. Equilibrium is reached for those samples with maximum Fe^{3+}/Fe^{2+} ratios (1.16±0.16) and minimum Mg# values.

4.4 Element and isotope compositions of noble gases

4.4.1 Fumaroles

Two dry gases were collected from a single high-temperature fumarole on the lower field at the base of Lastarria cone (5,030 m a.s.l.). The two samples yielded reproducible results (for He and Ne; Ar was analyzed in only one sample), which are presented in Table 3. In detail, the He concentrations were 9.6 and 10.8 ppm, while the Ne concentration was 0.06 ppm in both samples (the corresponding

$^{4}He/^{20}Ne$ ratios are 157 and 176). These results are comparable to those reported by Lopez et al. (2018) for samples obtained during the same sampling campaign. The ^{40}Ar concentration was 75 ppm, with an $^{40}Ar/^{36}Ar$ ratio of 315 (Table 3). He/Ne and Ar isotope data indicate the presence of moderate-to-severe air contamination, since the $^{40}Ar/^{36}Ar$ ratio remains slightly above the theoretical ratio in atmosphere ($^{40}Ar/^{36}Ar$=295.5; Ozima and Podosek, 2002). ^{40}Ar was thus corrected for air contamination ($^{40}Ar^{*}$) assuming that the ^{36}Ar present in our samples was derived from atmosphere, as follows:

$$^{40}Ar^{*}={}^{40}Ar_{sample} - ({}^{36}Ar_{sample}\times({}^{40}Ar/{}^{36}Ar)_{air})$$

The $^{3}He/^{4}He$ values corrected for atmospheric contamination (Rc/Ra) are 5.3 and 5.4 Ra (Figs. 5 and 6).

Fumaroles at Lascar volcano were not sampled in this study, and so below we only consider literature data for comparison with our measures in FIs.

4.4.2 Fluid inclusions

The concentrations and isotope ratios of noble gases in FIs are reported in Table 4. The LAS3 rock samples were the only ones from Lascar volcano where it was possible to hand pick sufficient olivines for measuring noble gases. The resulting noble-gas concentrations were 2.5×10^{-13} mol/g for He (Fig. 5), 1.1×10^{-14} mol/g for Ne, and 7.4×10^{-12} mol/g for Ar (Table 4). Cpx from the same sample showed a comparable amount of He (3.2×10^{-13} mol/g; Fig. 5) but higher Ne and Ar contents (5.8×10^{-14} and 9.2×10^{-12} mol/g, respectively), thus indicating greater air contamination. FIs from LAS1 Cpx xenocrystals from cumulates (see

Section 4.3.1) displayed He, Ne, and Ar ranges of concentrations of 2.0–2.9$\times$10^{-13}, 1.2–22.7$\times$10^{-14}, and 1.1–3.6$\times$10^{-12} mol/g, respectively (Fig. 5).

Among Lastarria samples, only in LRA3 it was possible to hand pick sufficient olivines for measuring noble gases; the other samples were analyzed for Cpx only. The He, Ne, and Ar concentrations in olivine FIs were 3.1$\times$10^{-13}, 5.6$\times$10^{-15}, and 3.7$\times$10^{-12} mol/g, respectively (Fig. 5, Table 4). FIs from Cpx in LRA2, LRA3, and LRA4 yielded He, Ne, and Ar concentrations of 0.2–6.6$\times$10^{-13}, 2.1–2.5$\times$10^{-14}, and 2.4–4.8$\times$10^{-12} mol/g, respectively (Fig. 5, Table 4).

The ^{4}He/^{20}Ne and ^{40}Ar/^{36}Ar ratios had ranges of 5.6–21.7 (Fig. 6) and 300–310, respectively, in Lascar samples, and of 1.0–55.4 (Fig. 6) and 302–308 in Lastarria samples. The ^{3}He/^{4}He ratios corrected for atmospheric contamination (Rc/Ra) vary between 6.9 and 7.3 Ra in olivines and Cpx from LAS1 and LAS3, while they are lower (5.2–5.4 Ra) in LAS1 Cpx xenocrysts (Fig. 5). Among Lastarria samples, the ^{3}He/^{4}He ratios vary between 5.3 and 8.0 Ra (Fig. 5). The ratio was highest for LRA3 olivines and lowest for LRA4 Cpx (Table 4). It should be noted that a strong atmospheric correction was found for LRA2 Cpx, with a marked difference between R/Ra and Rc/Ra (^{4}He/^{20}Ne=1.0). This sample has the lowest He content (2.4$\times$10^{-14} mol/g) and the lowest ^{4}He/^{40}Ar* (see Section 5.2.2), which could indicate diffusive fractionation of He from the crystal (e.g., Nuccio et al., 2008; Rizzo et al., 2018). Due to this possible secondary effect, we ignore this sample in the discussion below (see Table 4).

5. Discussion

5.1 Geothermobarometry of the plumbing system

We initially used pairs of mineral–liquid compositions to estimate the pressure/temperature (P/T) conditions of crystallizing magmas under the Lascar and Lastarria volcanoes. To achieve this aim we utilized major oxide concentrations as input parameters in different mineral–liquid equilibrium geothermobarometers (see Appendixes VI and VII, and below).

5.1.1 Lascar volcano

According to the estimated P/T conditions for magmas at Lascar, we propose a derived equivalent lithostatic pressure model with a minimum of three separate intrusive events occurring since ~9.5 ky. Each intrusion represents an ascending melt inside a crystal mush system (i.e. Marsh, 1995), keeping a magma chamber morphology is not conditional, but evolving vertically in the lithospheric crust. We assume those magmas have been following an isothermal decompression phase and a decompression/extended cooling phase, as observed in the P/T diagram (Fig. 7a). These two-step intrusive phases represent all sampled products (LAS1, LAS2, and LAS3) that crystallized magma with a two-pyroxene equilibrium for different storage zones and covering a depth of at least 41 km in the lithosphere (Fig. 7a).

Three mineral–liquid thermobarometer data sets were obtained for Cpx-Opx, clinopyroxene–liquid (Cpx-L), and orthopyroxene–liquid (Opx-L) pairs. In detail, the Cpx-Opx thermobarometer and mineral chemistry data indicate hypersthene and augite species at Lascar with compositions that are consistent with thermodynamic equilibrium at 642–649 MPa and 1079–1092 °C (Fig. 7a, Appendixes VI and VIII). The Cpx-L temperatures for Lascar are correlated with the pressure changes expressed by Equation 32d in Putirka (2008), ranging from 1067 to 1181 °C (1108±32 °C, n=8), while the range of Opx-L temperatures (Equation 28a in Putirka, 2008) is 875–1023 °C (913±70 °C, n=5).

The Cpx-L pair are in equilibrium for LAS1 output pressures between 305 and 546 MPa, except for LAS1 augite cumulates (xenoliths) that are chemically far from the Kd equilibrium and farther than the other mineral–liquid Mg# pairs (Fig. 4a). LAS1 hypersthene pressures reach 542 MPa, while the LAS2 scoriae reach 390 MPa (Fig. 7a). This is likely to correspond to maximum pressure conditions since none of these crystals have their rim composition in equilibrium with the surrounding glass. In LAS3, we infer pressures between 85 and 660 MPa for augite equilibrium, and its association with hypersthenes (as trapped solid inclusions) indicate that intergrowth of the two phases is possible under equilibrium conditions (Fig. 7a). For hypersthene and augite, we find an overall better Mg# equilibrium between the glass rim versus phenocryst rim compositions (Fig. 4a). Consequently, the crystallization sequence implies equilibrium of mafic minerals (Cpx or Opx) with the surrounding melts at depth between 4 and 22 km (Fig. 7). To illustrate the magmatic evolution that produced Cpx-Opx crystals, we thus propose the existence of an area with deep mafic magma reservoirs that would represent the ranges of lithostatic pressure depths shown in Fig. 10a. Lower pressure values (<305 MPa) would represent the plagioclase appearance controlled during the decompression cooling phase of the same ascending magma body (see Fig. 4a). This is likely to occur at shallower levels, possibly corresponding to the pounding zone illustrated in Fig. 10a.

Some peculiarities persist in the most-recent intrusive sequences. Regarding the mineral chemistry and glass compositions at Lascar, the 1986–1990 collapse of dome growth (LAS2) could represent distinct intrusive events, with magma being slightly more differentiated than for the 1993 explosive sequence (LAS1) (Fig. 10a). Crystals of dome growth also show Mg# heterogeneities, as evidenced by bimodal mafic mineral values (Mg# for olivine, hypersthenes, and augite; Fig. 3a). The 1989-1990 dome fragments represent a magmatic intrusive phase presumably with low cooling rates and longer residence time in the superficial 2-km-deep ponding zone below the central crater (Stechern et al., 2017). In contrast, the emitted scoria (LAS1) present in the pyroclastic flow of the 1993 eruption represents a direct and fast magmatic ascent.

Uncertainty also remains about the origin of trachitic-to-rhyolitic glass compositions probed on the mineral–glass pairs of our Lascar samples (Fig. 2a). This implies the possibility of encountering distinct intrusive events or residual differentiated melts that derive from a previous intrusive event (Fig. 10a). Such differentiated products have already been reported for emissions from the central crater and eastern vents of Lascar (Matthews et al., 1999; Gardeweg et al., 2011). For example, the range of glass compositions found in our study (Fig. 2) is close to the 1993 andesite scoria-dacitic pumice reported by Matthews et al. (1999), with SiO_2=62–65 wt%. In addition, white pumices with felsic compositions were found in the lithic-rich and pumice-rich lenses of the 1993 pyroclastic deposits (Sparks et al., 1997; Calder et al., 2000). Those evolved magmas probably reflect the trachitic-to-rhyolitic matrix glass compositions observed in the present study (e.g., SiO_2=72–73 wt%; Fig. 2a). We cannot exclude the possibility that those glasses result from extended differentiation from previous andesitic-to-dacitic magmas that intruded into the eastern Lascar edifice from 7.1 ky up to the present day.

5.1.2 Lastarria volcano

The three mineral–liquid thermobarometer data sets show that cooling/decompression behaviors affect Lastarria as they do Lascar (Fig. 7, Appendix VIII). Based on those results and the evolution of P/T parameters, we derived an equivalent lithostatic pressure model for the magmas that produced Ignimbrites 1 and 2 since ~4.85 ky A.P. (Fig. 10a). The most-recent Ignimbrite 3 (which is younger than ~2.46 ky) did not have mineral–liquid $Kd_{Fe\text{-}Mg}$ in equilibrium in our samples, and so its thermodynamic condition parameters were based on the data of Stechern (2017). No equilibrium pressures were encountered for LRA1 and LRA2, which were associated with Group C in Stechern et al. (2017) that corresponds to a source at a depth of ~20–40 km.

The detailed P/T data show hydrous Cpx-L pressures that are particularly variable at Lastarria, ranging from 989 MPa down to 199 MPa, with $Kd_{Fe\text{-}Mg}$ being in equilibrium (Fig. 7b, Appendix VIII). Hypersthenes are in equilibrium from 390 MPa down to <42 MPa at Lastarria (hydrous melts; Putirka, 2005, 2008; Lange et al., 2009). At Lastarria the Cpx-L temperatures are 1135–1147 °C (1140±38 °C, n=6), while those of Opx-L are 904–935 °C (921±13 °C, n=6). Many results for the tested Cpx-L and Plagioclase (Pgl)-L thermobarometric pairs follow vertical pressure decreases for relatively constant temperatures (isothermal decompression; Fig. 7, Appendix X).

Hypersthene, augite, and plagioclase species were found on thin sections and in the mineral chemistry analyses under various P/T conditions (Fig. 7b). Amphibole and biotite minerals were also identified, which support the presence of late crystallization conditions at superficial crustal levels at Lastarria (e.g., no amphibole present at depths >20 km according to Stechern et al., 2017). This indicates that magma evolution occurs at various depth ranges beneath Lastarria. The complex data related to the crystallizing magma reservoir beneath this volcano indicate that static magmas evolve both under deep and superficial conditions.

Overall, the data produced by this study support the frequent occurrence of mixing of variably differentiated materials in Lastarria magmas at different depth zones (up to 32 km) from >4.8 to 2.5 ky Ignimbrite sequences (Ignimbrites 1 and 2; Naranjo, 2010). Depth zones for mixing (e.g., Naranjo, 1992) with mafic endmembers were identified between 6.5 and 18 km by

Stechern et al. (2017), and they are supported by our data obtained from the mineral chemistry analyses and our observed mingling bands of clear and dark tones from LRA3 and LRA4 pumices. The scenario of mafic magma injection and mixing of different endmember compositions is supported by our scoria and pumice fragments of different ages (<4.8 ky), where inverse zoning is present in mafic minerals (Fig. 3b, d, f). This is evidenced in various single core–rim pairs of Mg# values of single phenocrysts (Appendixes II–V).

5.2 Primitive magma with stronger MORB signature modification at Lastarria volcano

The findings from the bulk-rock analyses of our samples were compared at Lascar and Lastarria volcanoes to verify the magma affinity and characterize the extent of differentiation from primitive magmas (Tables 1 and 2). Lascar volcano magmas show an Andean–continental-island-arc affinity for HFSE and transition-metal ratio (Sc/Ni) markers, while trace elements from Lastarria are typical of Andean magmatism in our samples (Fig. 8). The mafic origin of most Lascar products reflect a different type of magma differentiation, such as being less rich in K and corresponding to an homogeneous source, and so restricted to a typical volcanic arc signature (Fig. 8). The tectonic environment signature is similar, but even though the data set is very small, the La/Yb ratios clearly demonstrate that the cortical contribution is greater for Lastarria where elevation and crust thickness are expected to be greater (Thorpe et al., 1982; Hildreth and Moorbath, 1988; Stern, 2004). This highlights the common association with Andean K-rich magmas (Stern, 2004).

To verify if the MORB signature of magma was modified, bulk-rock results were plotted in a discrimination diagram where lines divide subduction from nonsubduction settings and arrows point to MORB and within-plate granite endmembers (Fig. 8b). The purple star in the figure indicating primordial mantle is from Bowden et al. (1984), which approximately divides ocean arcs from active continental margins. The evolution of K_2O/Yb versus Ta/Yb shows that both volcanoes emit products affected by fractional crystallization (Fig. 8b).

The concentrations of trace elements and REEs from bulk-rock analyses of both Lascar and Lastarria share familiar characteristics, such as both representing typical MORB and tholeiitic series. Since bimodal mantle and crustal magma origin are identified at Lastarria and are typical of Andean rocks, we suggest that various local factors can affect the bulk-rock chemistry and be superimposed over MORB signatures (Davidson and de Silva, 1992). The plate-rock enrichment in an intercontinental context probably reflects a certain mantle MORB signature modification at Lastarria via crustal contamination during episodes of magma stagnation (Fig. 8b). The composition variations are concordant with longer magmatic cycle pauses between Ignimbrites 1, 2, and 3, to at least three extrusive events occurring since ~4.9 ky (Naranjo, 2010). This chemical variation is far from reflecting large-volume Andean ignimbrites emitted during long-term tectonic cycles covering millions of years (e.g., de Silva et al., 2006; Scott et al., 2018; Wörner et al., 2018), and so bulk-rock chemistry contamination at the scale of the vertical plumbing system may represent basement heterogeneities (Wörner et al., 1994; Haschke et al., 2006).

At Lascar this dual chemical characteristic is not present in the magmas that has intruded into the crust since ~9.5 ky, at least for the samples analyzed in the present study, since Fig. 8 shows a typical volcanic arc signature with a lower cortical influence (low K_2O/Yb and La/Yb ratios). The chemistry of bulk rock represents a less-contaminated composition of one particular major magmatic cycle during the 1980s and 1990s and an older volcanic event from the Holocene. This extent of MORB modification from Lascar magma probably represents shorter residence times for the “crystal mush” systems modeled in Fig. 10.

5.3 Geochemistry of fumarole gases and FIs

5.3.1 Atmospheric contamination

The $^{4}He/^{20}Ne$ and $^{40}Ar/^{36}Ar$ ratios of fumarole gases and FIs highlight a variable extent of air contamination. Fumarole gases from Lastarria and Lascar display the minor addition of air relative to FIs, as indicated by their higher $^{4}He/^{20}Ne$ (Fig. 6) and $^{40}Ar/^{36}Ar$ (Tables 3 and 4) ratios. This suggests that FIs were entrapped by recycled fluids in contact with the atmosphere, such as mixing with water that circulates in the form of conductive hydrothermal cells in contact with intrusive magmas (Fig. 10). It is more likely that FIs entrapped air under posteruptive conditions (during magma cooling) via mineral fractures (Nuccio et al., 2008).

The $^4He/^{20}Ne$ and $^{40}Ar/^{36}Ar$ ratios measured in fumarole gases from Lascar and Lastarria volcanoes are far from typical MORB-like values ($^4He/^{20}Ne$>1000 and $^{40}Ar/^{36}Ar \leq 44{,}000$; e.g., Burnard et al., 1997; Ozima and Podosek, 2002). This indicates that an atmospheric component is involved in the local magmatic and/or mantle source. These ratios actually fall within the range of values measured in other arc volcanoes worldwide (Hilton et al., 2002; Shaw et al., 2003, 2006; Martelli et al., 2014; Di Piazza et al., 2015; Rizzo et al., 2015; Robidoux et al., 2017; Battaglia et al., 2018). This evidence reinforces the idea that atmospheric components are also recycled into the mantle by subducting slabs.

5.3.2 Inferences on the mantle sources beneath Lascar and Lastarria volcanoes

We evaluated the geochemical features of magmatic/mantle sources beneath Lascar and Lastarria by focusing on $^3He/^4He$ corrected for air contamination (Rc/Ra). We also considered $^4He/^{40}Ar^*$, when available, because this parameter can track magmatic degassing in phenocrysts and fumaroles. This is because He is around 10 times more soluble than Ar in silicate melts, although this difference can vary due to the chemistry and pressure of magmas, leading eventually to $^4He/^{40}Ar^*$ increasing especially during the late stages of degassing (e.g., Iacono-

Marziano et al., 2010; Boudoire et al., 2018). It should be noted that the $^{4}He/^{40}Ar^{*}$ ratio in the upper mantle is typically within the range of 1–5 (Marty, 2012).

As reported in Sections 4.4.1 and 4.4.2, the cogenetic olivine and Cpx from LAS1 and LAS3 show Rc/Ra values between 6.9 and 7.3 Ra, while Cpx xenocrysts of LAS1 display lower values of 5.2–5.4 Ra(Figs. 5 and 6). The $^{3}He/^{4}He$ ratios measured in LAS1 and LAS3 phenocrysts are comparable to the range of values measured in fumarole gases by Tassi et al. (2009) (6.5–7.3 Ra), suggesting that fumarole gases from Lascar are representative of the local magmatic source (see Fig. 10a) and do not experience any shallow contamination (e.g., in the hydrothermal system) by crustal-derived ^{4}He. Instead, the lower value measured in Cpx xenocrysts from LAS1 probably reflects contamination by crustal-derived ^{4}He, which is accentuated by the low $^{3}He/^{4}He$ values of xenocrysts from LAS1; this result for a magma that differentiated and degassed over a long time period favors the production and accumulation of radiogenic ^{4}He from basement rocks. This hypothesis is reasonable since LAS1 xenocrysts represent augite cumulates that may have experienced a lower cooling rate and a longer residence time for the dome fragment formed during 1989-1990. This idea is qualitatively supported by the $^{4}He/^{40}Ar^{*}$ ratio, which is lower ($^{4}He/^{40}Ar^{*}$=1.2–2.1) in samples displaying the highest $^{3}He/^{4}He$ ratios (LAS1 and LAS3) than in xenocrysts from dome fragment LAS1 ($^{4}He/^{40}Ar^{*}$=5.0–6.0).

In the case of Lastarria volcano, FIs showed $^{3}He/^{4}He$ ratios between 5.3 and 8.0 Ra (Figs. 5 and 9). The highest value (8.0 Ra) was uniquely measured in the olivine of LRA3, while lower values (5.3–6.6 Ra) were measured in Cpx of

LRA3 and LRA4, which represent Ignimbrites 1 and 2 (Table 4). The fumarole gases analyzed in this work have a mean $^{3}He/^{4}He$ ratio of ~5.3 Ra, which is within the range of previous fumarole measurements (4.6–6.2 Ra) by Aguilera et al. (2012) and Lopez et al. (2018) (Figs. 5 and 10b). We argue that FIs of olivine reflect a more-primitive signature of $^{3}He/^{4}He$ than Cpx and fumarole gases. These latter samples seem to reflect a later (shallower) stage of magma degassing before the series of ignimbrites is produced (Fig. 10b), with sizeable crustal contamination by crustal-derived ^{4}He in the shallower parts of the volcano plumbing system. The evidence from petrography and mineral chemistry indicates multistep ponding of magmas that could explain the observed variability in $^{3}He/^{4}He$ ratios between olivine and Cpx.

In order to draw conclusions about the local mantle source, we consider the highest $^{3}He/^{4}He$ values measured in FIs from Lascar and Lastarria. The $^{3}He/^{4}He$ value of 7.3 Ra measured in FIs from Lascar falls within the lower end of the MORB range (8±1 Ra; Graham, 2002), while that of 8.0 Ra in FIs from Lastarria is around the middle of the MORB range (Figs. 5 and 6). These values fall within the range of typical ratios reported for some volcanic arc segments worldwide independently of sediment contributions or the presence of a serpentinized oceanic plate (e.g., central and northern Chile, Peru, and Ecuador, Kamchatka, and the Kuriles Island; Hilton et al., 2002; Völker et al., 2013; Jacques et al., 2014). Nevertheless, recent studies of $^{3}He/^{4}He$ in FIs from rocks erupted in the Central American Volcanic Arc (CAVA) suggest that slight but appreciable differences (of 0.5–1.0 Ra) could reflect contamination of the source by subducting sediments bearing U and Th (Di Piazza et al., 2015; Robidoux et al., 2017; Battaglia et al., 2018). This means that the mantle beneath Lastarria is either not contaminated or is less contaminated than that beneath Lascar, as observed in other arc volcanoes of the CAVA (Turrialba and Pacaya; Di Piazza et al., 2015; Battaglia et al., 2018). An alternative explanation is that the magmatic dynamics are more active beneath Lastarria than Lascar, and the $^3He/^4He$ difference between the volcanoes is attributable to crustal contamination.

More generally, the $^3He/^4He$ ratios measured in FIs from Lascar and Lastarria are higher than the maximum values reported for central and northern Chile (6.84 and 6.02 Ra, respectively; Hilton et al., 1993) and comparable to the highest values measured in the Planchón-Peteroa volcano (7.1 Ra; Tassi et al., 2016) and the Copahue-Caviahue volcano (7.9 Ra; Agusto et al., 2013) located in southern Chile. Another consideration that arises from this and past studies of $^3He/^4He$ in South America is that only fumarole gases from very active volcanoes (i.e., strongly degassing SO_2 into the atmosphere) and FIs in olivine and pyroxene yield values that can be used for extrapolations to mantle features. Instead, $^3He/^4He$ ratios measured in geothermal fluids and fumaroles from volcanoes exhibiting little activity (with no active SO_2-rich plume) or quiescent volcanoes (e.g., Hilton et al., 1993; Ray et al., 2009; Benavente et al., 2016; Tassi et al., 2016 and references therein) are always below the MORB range, indicating variable extents of crustal contamination (Fig. 9). These extents of contamination seem also to be related to how far the gas emissions are from the arc front. For example, the fumaroles (n=3) sampled farthest from the active volcanic front fall below the (uncorrected) Ra range of 0.82–6.02 (2.39±1.43) reported for northern Chile by Hilton (2002). Contrary to central Chile where Ra progressively increases from north to south with a decreasing contribution from continental crustal ^{4}He (Benavente et al., 2016), there is no clear north–south variation or a correlation between the values in Peru and northern Chile (Fig. 9). This Ra variation instead decreases as the thickness of the rigid continental crust increases toward the east of the Andean cordillera (Gardeweg et al., 2011).

6. Conclusions

According to the petrological data from bulk rocks and mineral separates (olivine, ortho-Cpx, and plagioclase) from andesite scorias, the post-1989 Lascar reservoir is fed by a single intrusive event of mafic magmas that bypassed various differentiated magma supplies (potentially magma ponding zones with rhyolitic compositions represented by the pumice rocks; Matthews, 1994; Matthews et al., 1999). A similar scenario may produce the andesitic Tumbres flow, but at the beginning of the Holocene (Gardeweg et al., 2011). Intrusive magmatic bodies are drained in ponding zones at distinct crustal depths identified with P/T models as crystallizing Opx equilibrium ranges (390–649 MPa, corresponding to lithostatic equivalent depths [LEDs] of 15–21 km). The magmas ascend rapidly through the crust until reaching a shallow ponding zone where Cpx and plagioclases are in equilibrium (from <305 to 741 MPa, corresponding to

LEDs ranging from 12–29 km up to 3.4–6.7 km). In contrast, Lastarria is fed by multiple intrusive events (Ignimbrites 1, 2, and 3) that originally took shape under the deepest crustal conditions illustrated by our data set (~500–990 MPa, corresponding to LEDs of ~20–40 km) that encompass the petrological range of values estimated by Stechern et al. (2017). We have identified the minimum depth crustal zones for residual crystallizing magma to equilibrate mafic minerals as 6.5–8 km, which is consistent with Stechern et al. (2017). A superficial mixing zone from 1 to 5–6 km appears to receive the most-differentiated magmas and residual fluids that could explain deformation detected by interferometric synthetic-aperture radar as well as tomographic seismology anomalies (Remy et al., 2014; Diaz et al., 2015; Spica et al., 2015). Overall, the various magma storage levels at Lastarria represent magmatic cycles affected by mixing effects, with inverse zoning from phenocrysts exerting different affects in each distinct magmatic event).

We now combine the information on plumbing system depths with isotope data of noble gases measured in fumaroles and FIs from mafic minerals that represent residual magmatic fluids. The two studied stratovolcanoes have distinct parental magma compositions despite the similarities in their explosive volcanic behaviors and geological backgrounds. The Lascar magmatic fluids and parental magma showed some degree of air contamination, with $^{40}Ar/^{36}Ar$=300–310 and $^{4}He/^{20}Ne$=5.6–204. The $^{3}He/^{4}He$ ratios (6.91–7.12 Ra) from minerals in scoria from any ages (the Tumbres flow in 1993) are homogeneous and slightly lower than those for a MORB-like magmatic source (8±1 Ra; Graham, 2002), suggesting that one type of parental magma is ascending below Lascar independently of the emission sites and crystallization mechanisms. Magmas with longer residence times would necessarily experience lower cooling rates of the crystallizing plug and allow more time for the absorption of more radiogenic ^{4}He, such as via crustal contamination after mixing with pristine MORB-like fluids.

The Lastarria magmatic fluids and parental magma also show some degree of air contamination, with ^{40}Ar/^{36}Ar=302–308 and ^{4}He/^{20}Ne=1.0–55.4. Olivine FIs trapped the most-primitive fluids (8.01 Ra), highlighting the sequence of fractional crystallization between Cpx and olivine phenocrysts (Shaw et al., 2003, 2006). The ^{3}He/^{4}He ratios show significant variability of 5.31–8.01 Ra. In this situation we cannot exclude that fluids trapped in olivine reflect different plumbing systems conditions, which could support the hypothesis of crustal contamination by the addition of radiogenic ^{4}He; this is probably a common feature below the Lascar and Lastarria edifices considering the large crustal thickness below the CVZ (Trumbull et al., 1999). Bulk-rock traces and REE signatures provide evidence of differentiation and one short magmatic cycle that crystallizes a single type of mantle MORB magma, but the signature is strictly related to volcanic arc features at Lascar (e.g., La/Yb and U/Th values). A high degree of compositional heterogeneity was observed in the bulk-rock data for Lastarria, with variable noble-gas signatures between the distinct magmatic events.

Supplementary data (Appendixes I–X) related to this article can be found online.

Acknowledgments

We thank the INGV laboratory staff for providing access and analytical support. We also thank the DiSTeM laboratory at the University of Palermo for supporting this work with internship opportunities at INGV. Special thanks are due to Mariano Tantillo and Mariagrazia Misseri for helping in sample preparation and noble-gas analyses, as well as to Piergiorgio Scarlato for allowing access to the HPHT laboratory of INGV in Rome for electron microprobe analysis. We also would like to mention the field participation of Universidad Católica del Norte in Antofagasta and the organizer of the 2014 IAVCEI CCVG 12th Volcanic Gas Workshop in Chile, who made access possible for field rock sampling; that workshop also provided a student travel scholarship of US$ 1,000. This work was partially supported by the Deep Carbon Observatory.

Table and figure captions

Table 1 – Locations.

Listing of sample coordinates along with field and sample petrographic descriptions.

Table 2 – Bulk-rock analyses.

Bulk-rock major-element compositions were analyzed for major elements, trace elements, and REE using a combined ICP/MS device (WRA4B2) at Ancaster (Code 4B2-Std, Actlabs). Results of bulk-rock analyses of powder samples prepared at the DiSTeM laboratory at the University of Palermo. The measurement detection limits are also listed.

Table 3 – Chemical and isotope compositions of noble gases from fumaroles.

*UTM Zone 19 (S) at an altitude of 5030 m a.s.l.

Table 4 – Chemical and isotope compositions of noble gases from FIs.

*Sample with an xenocrystal origin.

Figure 1 – Locations. Topographic map and locations of the analyzed volcanoes. (a) Converging Nazca and South America plates (Nazca/SAm) with its subduction vector illustrated using a black arrow representing the NUVEL 1-A model from DeMets et al. (1994). (b) Continental-scale map showing the North Volcanic Zone (NVZ), CVZ, and South Volcanic Zone (SVZ).

Figure 2 – Rock classification according to Peccerillo and Taylor (1977). Diagram of K_2O versus SiO_2 for bulk-rock compositions in this study and mineral glass rims and bulk-rock compositions in the literature. Compositional data are for (a) Lascar and (b) Lastarria.

Figure 3 – Frequency diagrams of Mg#. Core and rim Mg# values provided for each crystal in the studied rock samples from Lascar (LAS1, LAS2, and LAS3) and Lastarria (LRA2, LRA3, and LRA4). (a) Hypersthene from Lascar, (b) hypersthene from Lastarria, (c) augite from Lascar, (d) augite from Lastarria, (e)

olivine from Lascar and Lastarria, and (f) plagioclase An# contents from Lascar and Lastarria.

Figure 4 – Crystal versus liquid compositions. Mg# values for liquid (glass) are compared to Mg# values for minerals (hypersthenes and augite are indicated by colored squares and lozenges, respectively). Equilibrium mineral–glass (total Fe) values are plotted along with data from the literature. The results indicate Fe^{2+} (fully black symbols: hypersthenes and augites are indicated by squares and lozenges, respectively). Data are for (a) Lascar and (b) Lastarria.

Figure 5 – $^{3}He/^{4}He$ ratios corrected for atmospheric contamination (Rc/Ra) versus He concentration in FIs. Typical ratios from MORB are 8±1 Ra (Graham, 2002). Ranges of published $^{3}He/^{4}He$ values for fumaroles are from Tassi et al. (2009) for Lascar and Aguilera et al. (2012) for Lastarria.

Figure 6 – $^{3}He/^{4}He$ versus $^{4}He/^{20}Ne$ in fumaroles and FIs. Symbols are as indicated in Fig. 5.

Figure 7 – Geobarometers. Graphs of estimated P/T relationship for magma crystallization conditions. The geobarometers include Opx-L and Cpx-L pairs from Putirka et al. (2003) and Equation 32c in Putirka (2005) are plotted for Lascar and Lastarria data sets. The Cpx-Opx thermobarometer data are compared when mineral pairs are observed in rock samples (Equations 38 and 39 in Putirka et al., 2008). Data sets for plagioclase-liquid pairs (Lange et al., 2009) are illustrated with water contents of the liquid melt system listed in Appendix VI and VII. The water contents are only known at Lastarria from hygrometer estimates (H_2O=1–2.1 wt%) and the solubility model of Newman and Lowenstern (2001). Cpx and Opx versus liquid equilibrium geobarometers are estimated in dry and wet conditions (Putirka, 2003, 2005, 2008). Amphibole pressures and temperatures from Stechern et al. (2017) were obtained using Ridolfi et al. (2010) for amphibole (1) data, and Ridolfi and Renzulli (2012) for amphibole (2) models. Data are for (a) Lascar and (b) Lastarria.

Figure 8 – Rock classification diagram. Results from Lascar and Lastarria bulk-rock chemistry analyses. (a) Tectonic discrimination of the andesites (Bailey, 1981). The tectonic discrimination diagrams of La/Yb versus Sc/Ni are from Bailey (1981), which provide evidence for each tectonic environment while highlighting the common association with Andean magmas. HFSE Sc versus transition-metal Ni marker for a mafic origin. b) Tectonomagmatic environment (Bowden et al., 1984). Diagram of K_2O/Yb versus Ta/Yb where the tectonomagmatic environment provides evidence from the discrimination diagrams of Bowden et al. (1984) reporting Yb (LREE). Lines divide subduction from nonsubduction settings and arrows point to MORB and within-plate granite (WPG) endmembers. The purple star indicating primordial mantle is from Bowden et al. (1984), which approximately divides ocean arcs from active continental margins; central Andes and volcanic arc basalts are also from that study. Shoshonitic (SHO), CA, and tholeiitic (TH) series are shown to also be consistent with mobile major-element diagrams in the other figures. Vectors on the right-hand side indicate different factors that may affect the bulk-rock distribution. Literature samples are from Deruelle (1982), Matthews et al. (1994), Naranjo (1992), Wittenbrink (1997), Matthews et al. (1999), Rosner (2003), and Mamani et al. (2010).

Figure 9 – Spatial distribution of Rc/Ra in northern Chile. The locations of volcanoes are shown with black triangles. Lascar and Lastarria are indicated by blue triangles with black centered dots. The symbols for different ranges of Rc/Ra values of fumarole samples are explained in the legend.

Figure 10 – Derived equivalent lithostatic pressure model for ascending magmas. $^3He/^4He$ ratios corrected for atmospheric contamination (Rc/Ra) are associated with magma intrusion events at (a) Lascar and (b) Lastarria.

List of Appendixes

Figure1
Click here to download high resolution image

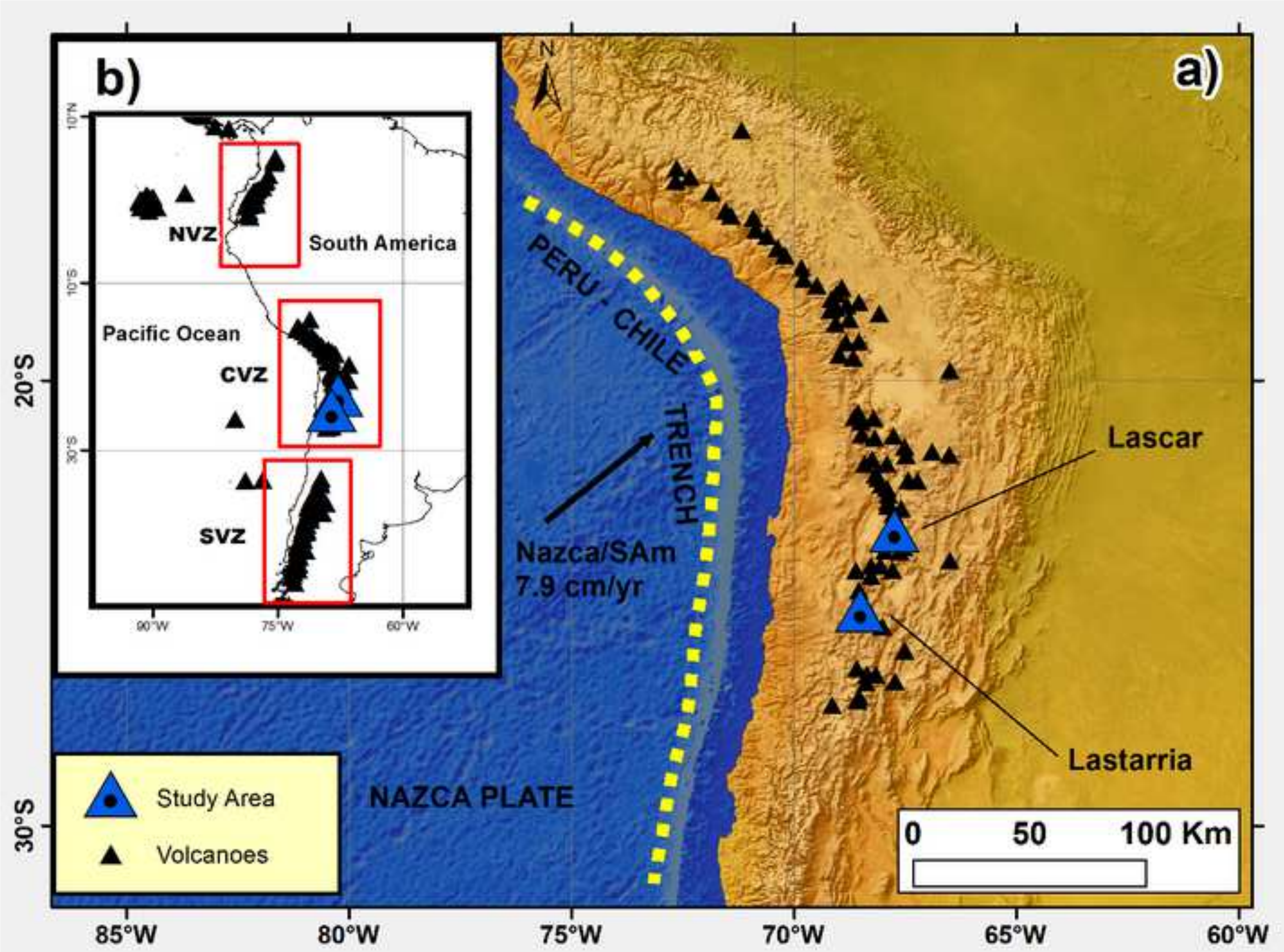

Figure2
Click here to download high resolution image

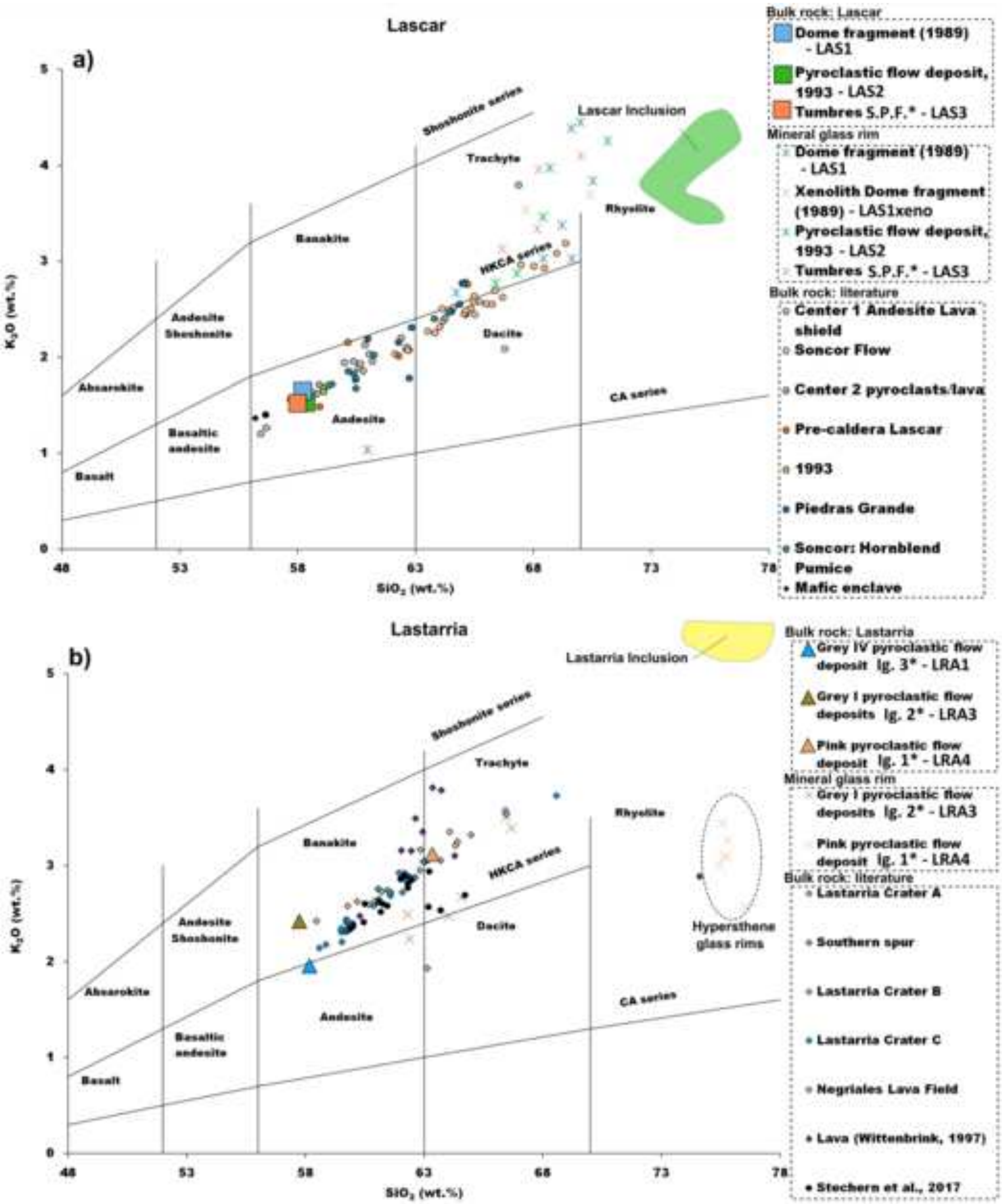

Figure3

Click here to download high resolution image

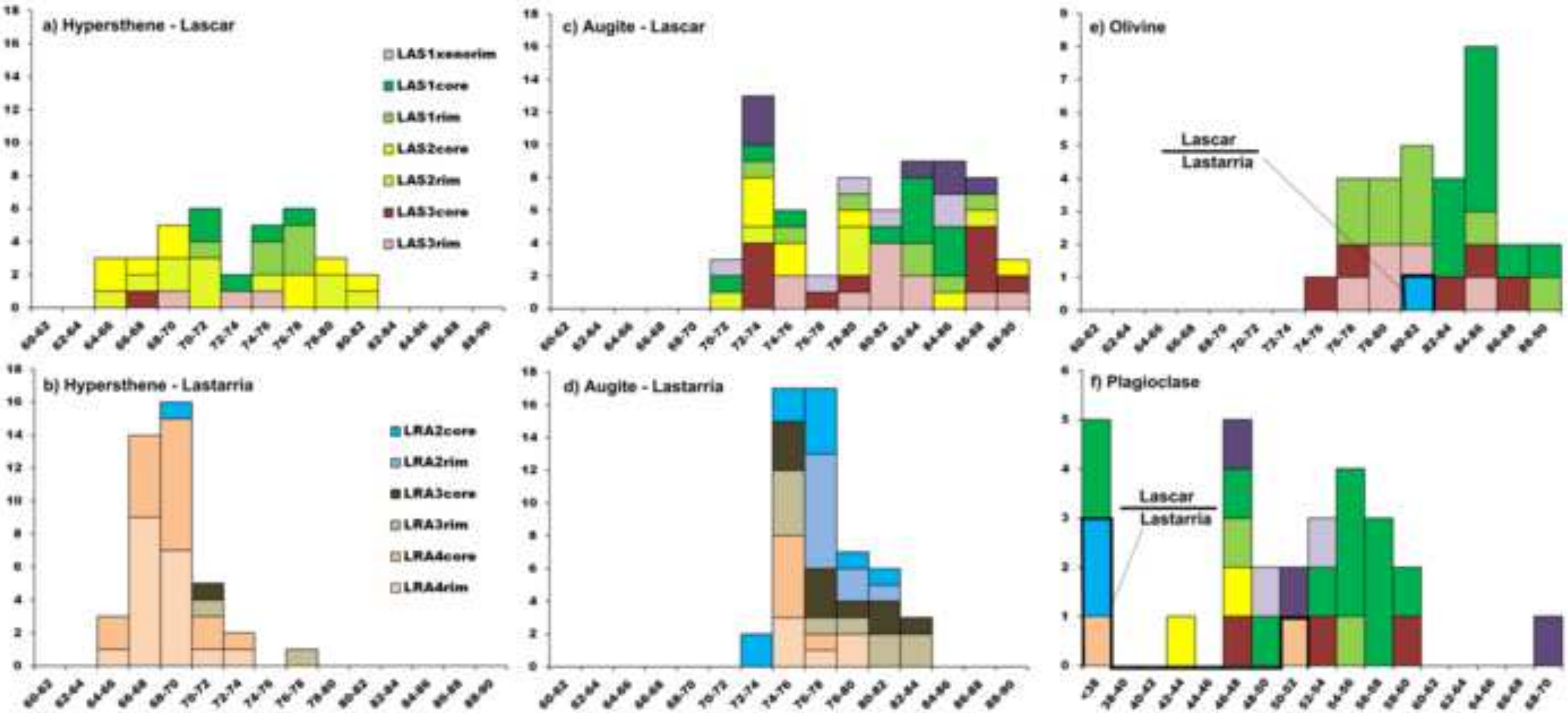

Figure4
Click here to download high resolution image

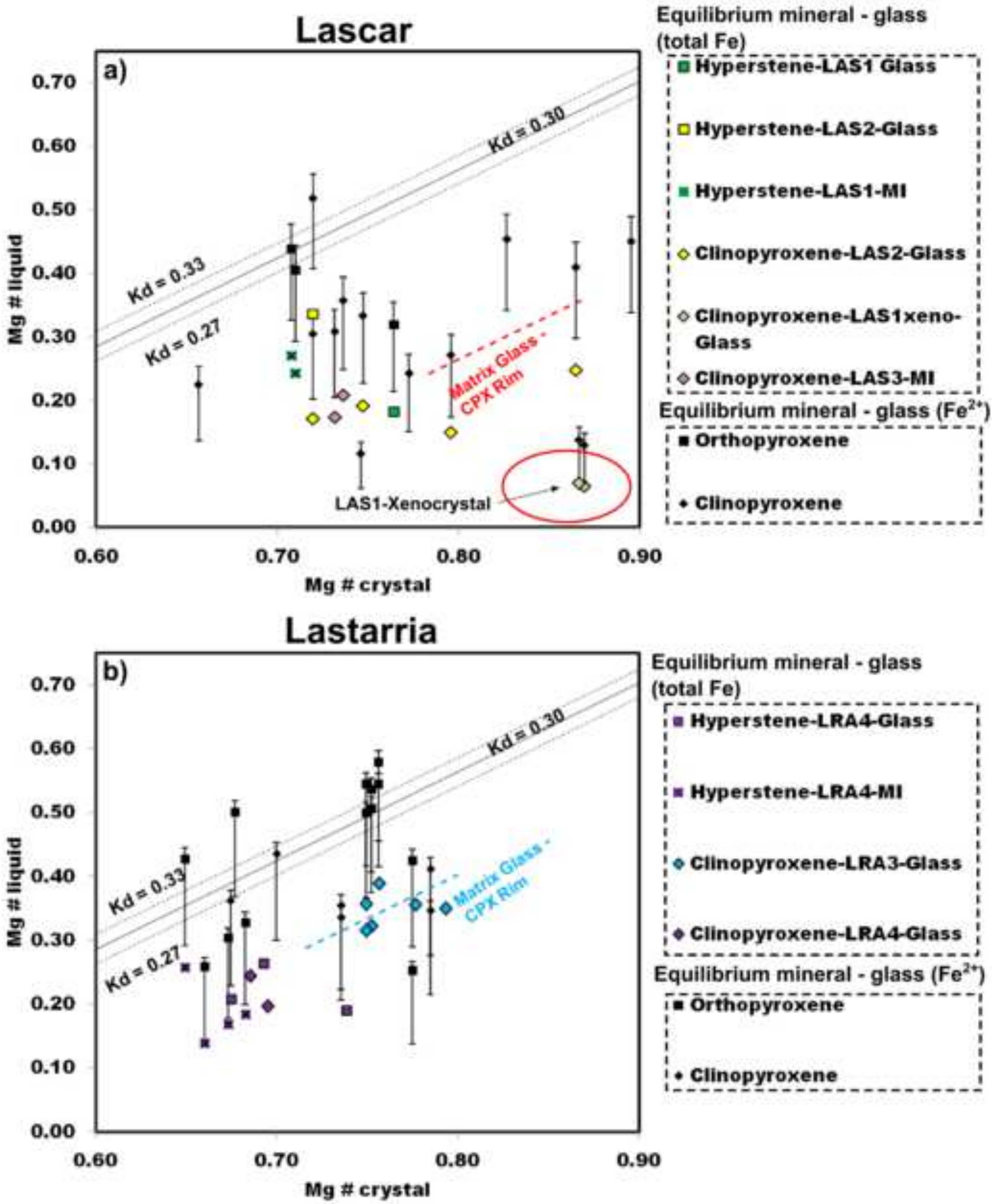

Figure5
Click here to download high resolution image

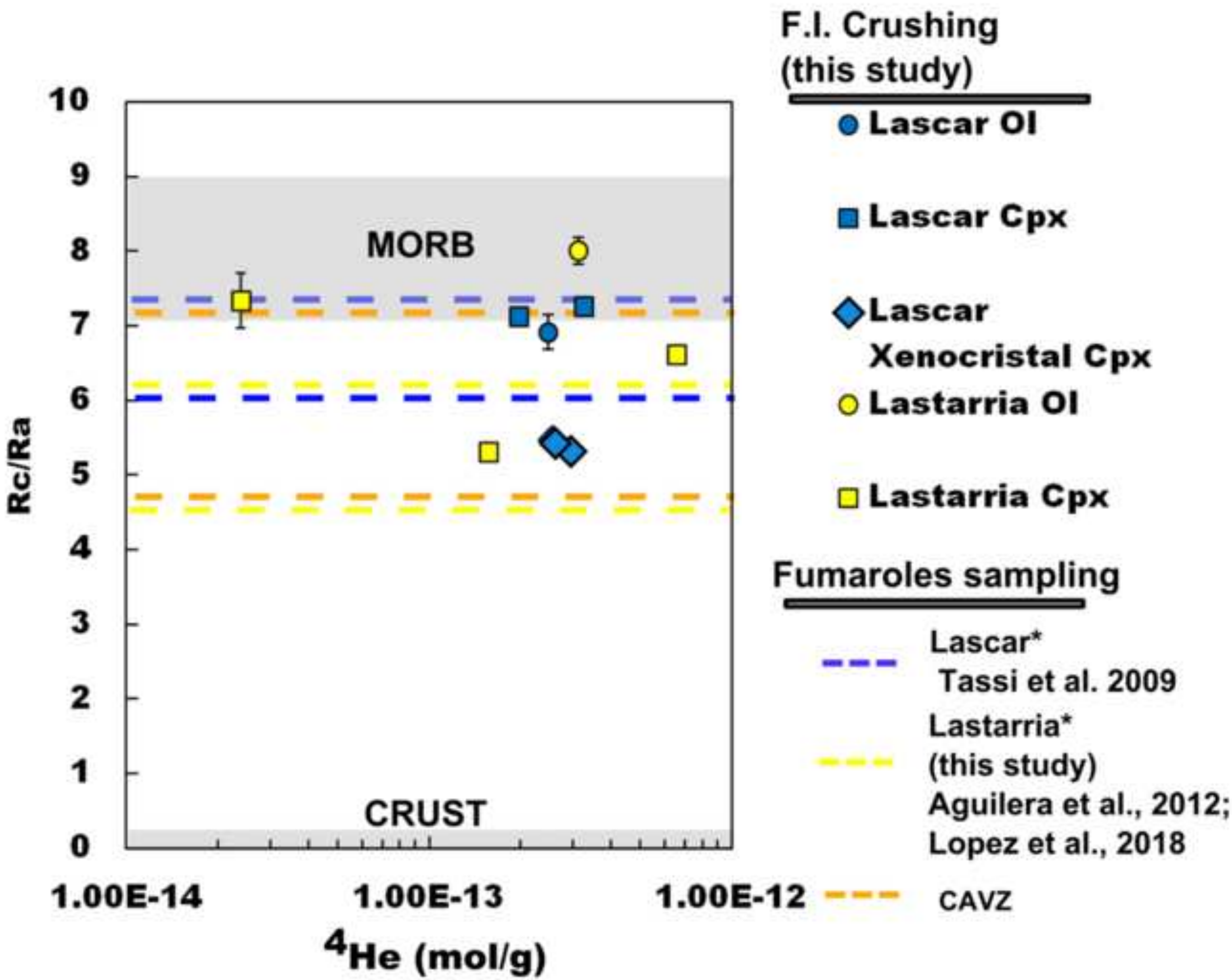

Figure6

Click here to download high resolution image

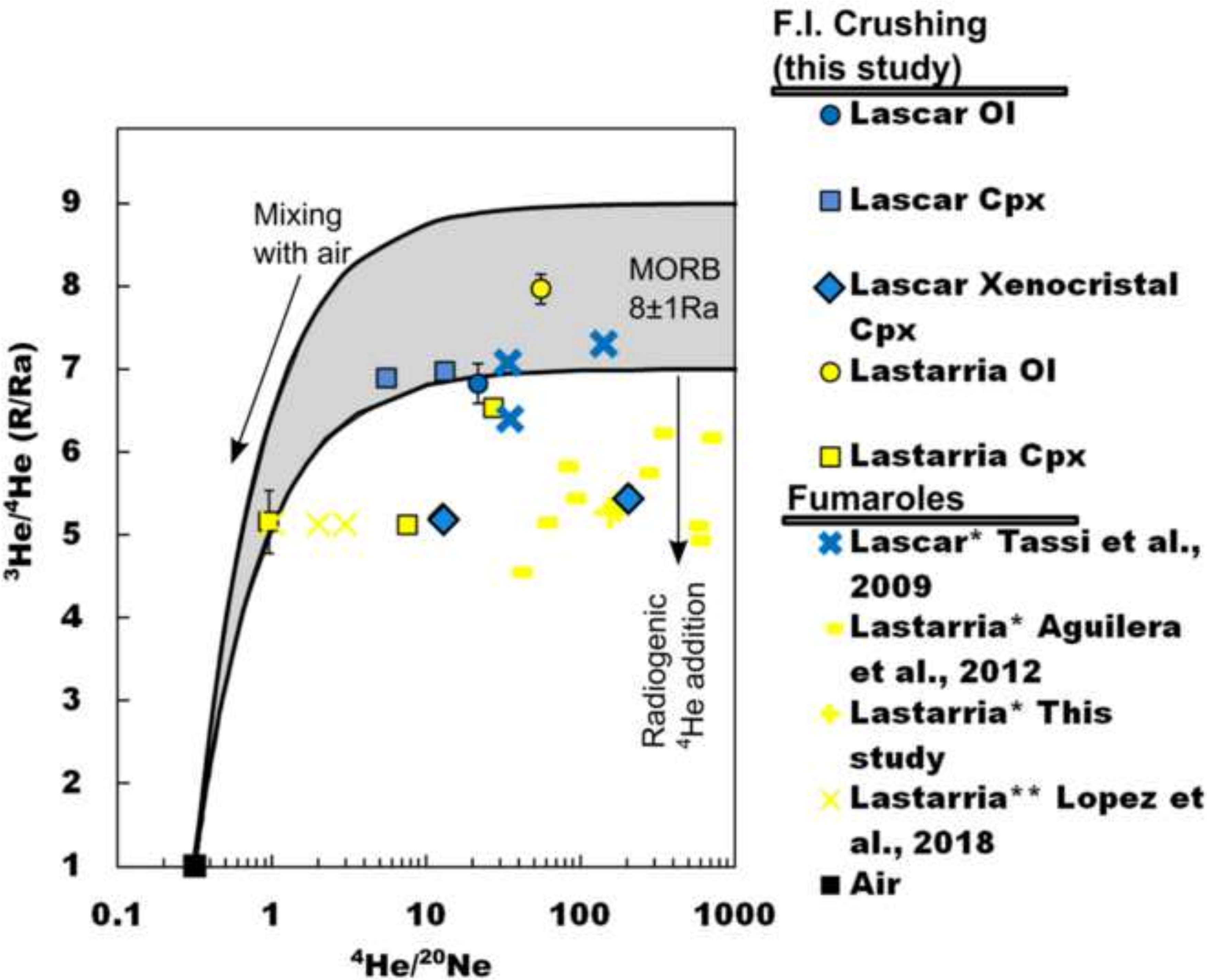

Figure7
Click here to download high resolution image

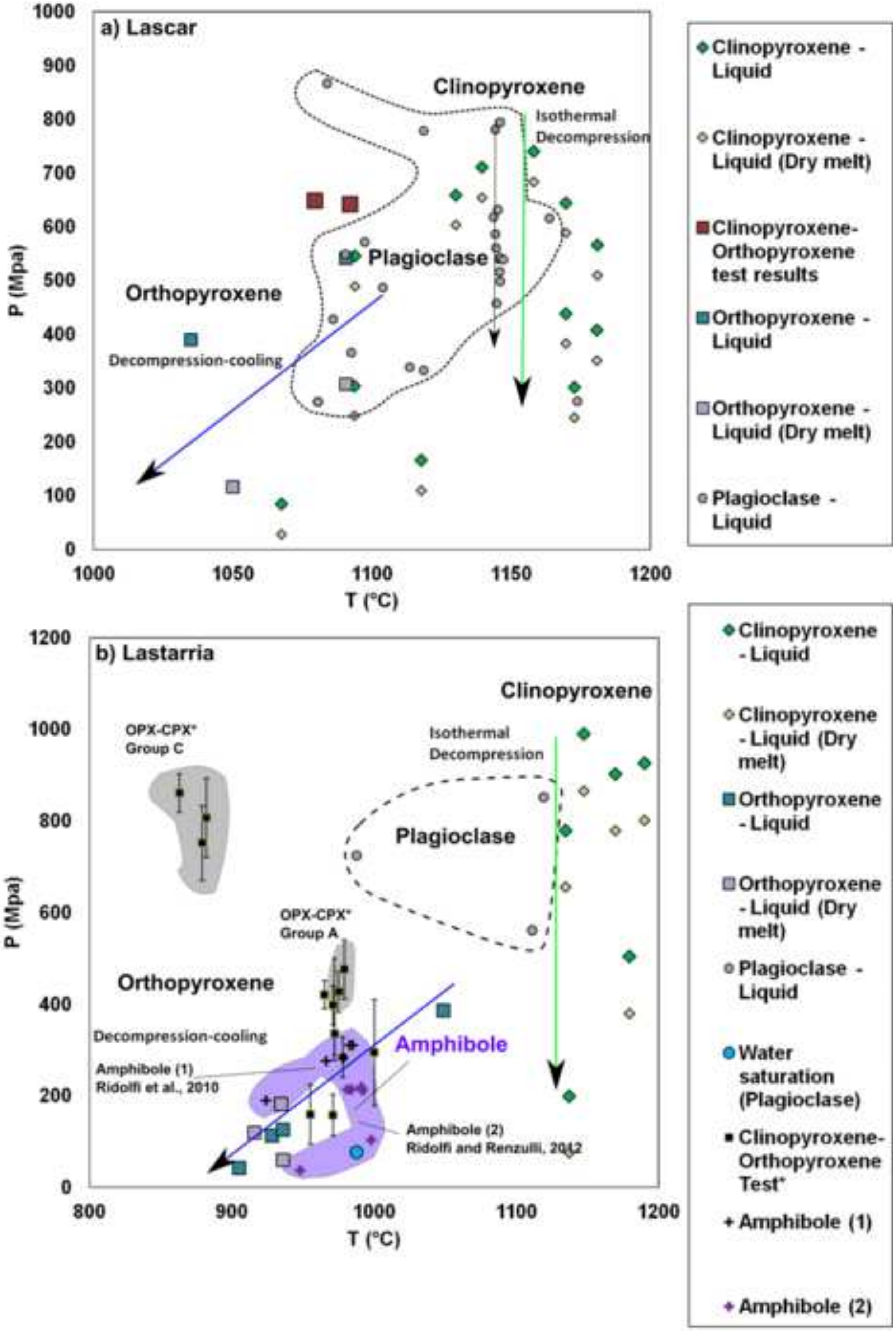

Figure8
Click here to download high resolution image

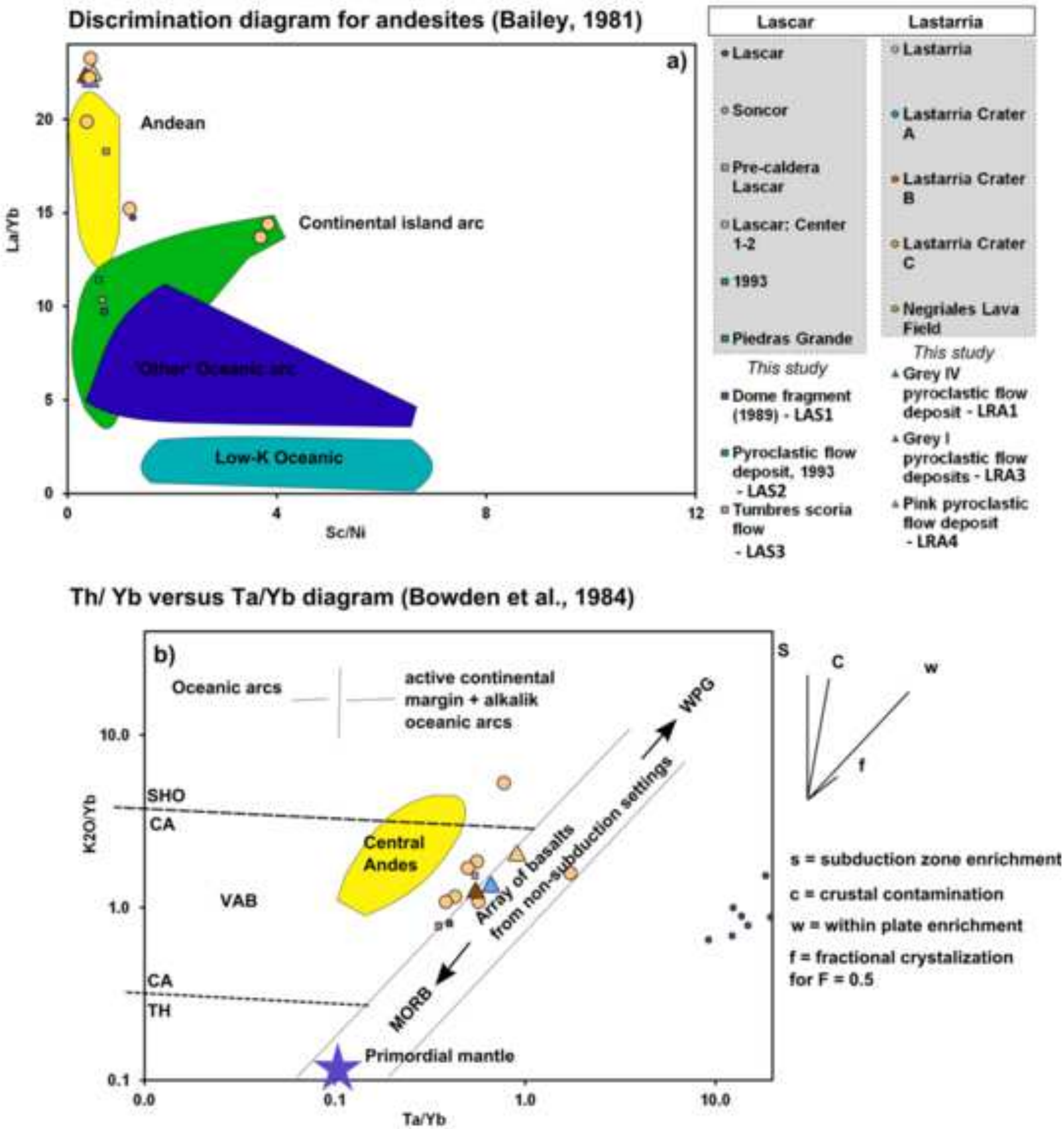

Figure9

Click here to download high resolution image

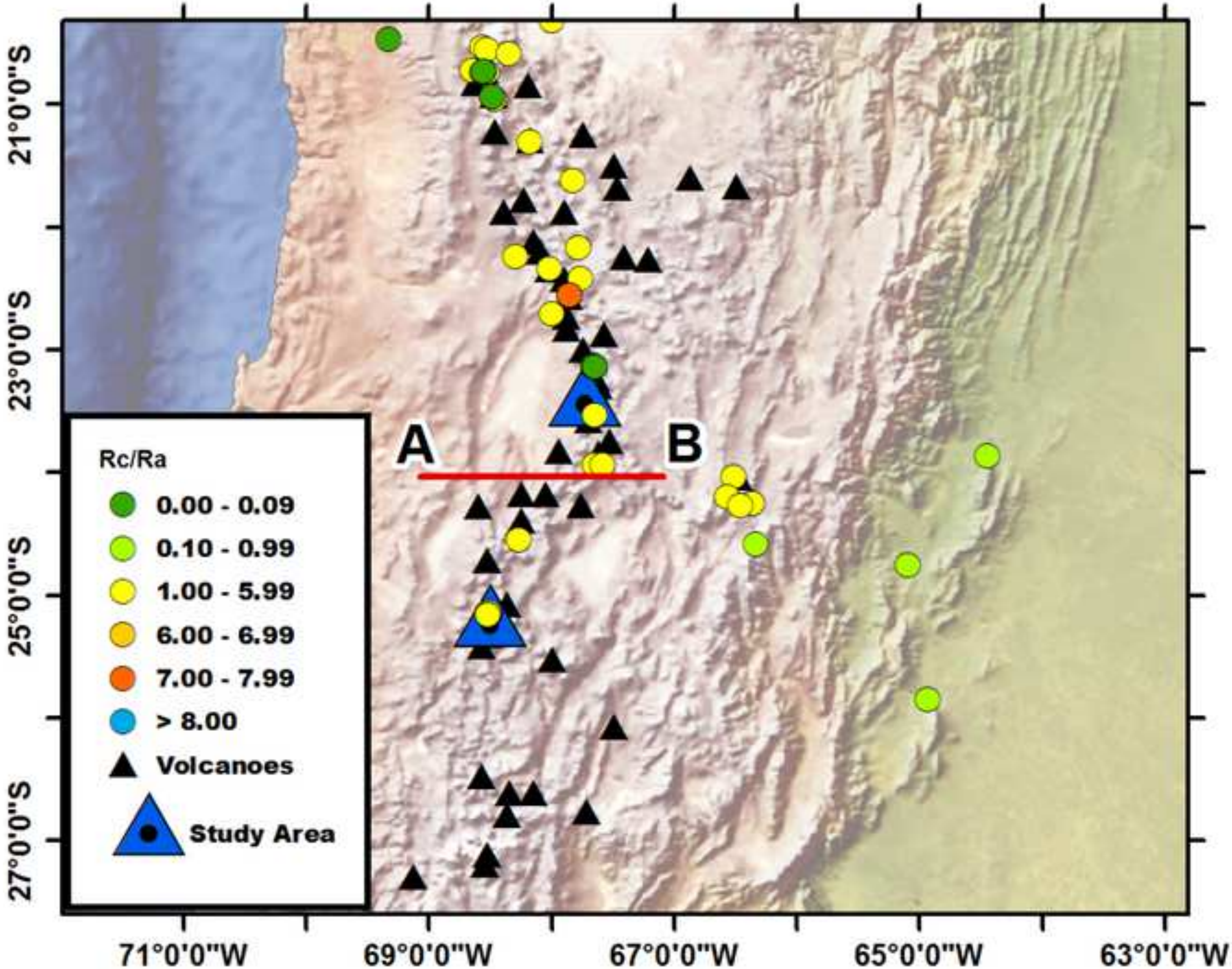

Figure10

Click here to download high resolution image

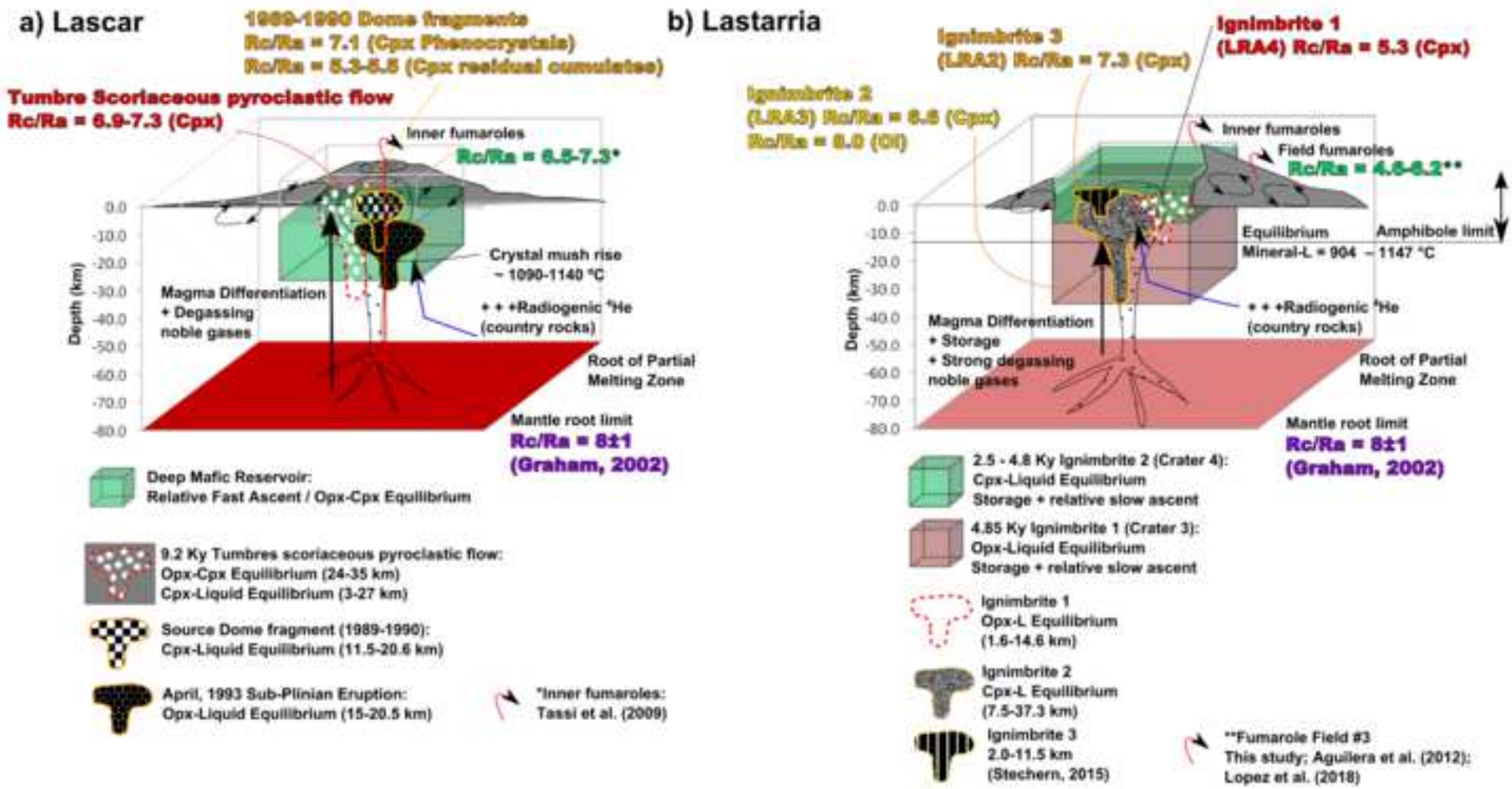

Table1
Click here to download Table: Table 1.xlsx

Table 1 – Sample description

Sample ID	Volcano	Long (deg.)	Lat (deg.)	Alt. (m)	Material
LRA1	Lastarria	25° 9'17.11"S	68°31'32.36"O	4992	Escoria Block
LRA2	Lastarria	25° 9'17.11"S	68°31'32.59"O	4992	Escoria Block
LRA3	Lastarria	25° 8'31.437''S	68° 31'47.579''O	4697	Pumice fragments
LRA4	Lastarria	25° 8'12.814''S	68° 32'7.793''O	4558	Pumice fragments
LAS1	Lascar	23° 18'46.605''S	67° 47'0.67''O	3919	Dome fragment
LAS2	Lascar	23° 18'45.09''S	67° 47'2.197''O	3925	Escoria Block
LAS3	Lascar	23° 18'59.843''S	67° 47'48.253''O	3890	Escoria Block

[a] *Aguilera (2008)*

[b] *Dome fragment emitted inside 1993 pyroclastic flow*

Table2
Click here to download Table: Table 2.xlsx

Table 2 – Chemical compositions of bulk rock

Sample		LAS1	LAS2	LAS3	LRA2
Volcano		Lascar	Lascar	Lascar	Lastarria
Material		Dome fragment (1989)	Escoria Block	Escoria Block	Escoria Block
SiO_2 (wt.%)	0.01	57.86	58.2	57.39	58.06
Al_2O_3	0.01	16.75	16.17	16.04	16.88
Fe_2O_3(T)	0.01	7.11	7.62	7.49	7.36
MnO	0.001	0.124	0.123	0.125	0.114
MgO	0.01	4.39	4.26	4.61	4.22
CaO	0.01	7.17	7.18	7.2	6.74
Na_2O	0.01	3.36	3.49	3.39	3.34
K_2O	0.01	1.61	1.57	1.54	1.95
TiO_2	0.001	0.724	0.821	0.776	0.979
P_2O_5	0.01	0.18	0.31	0.24	0.21
LOI		n.d.	0.3	0.14	0.7
Total		99.21	100	98.95	100.6
Sc (ppm)	1	21	18	20	14
Be	1	2	2	2	2
V	5	168	175	174	153
Ba	2	371	378	367	426
Sr	2	469	572	524	554
Y	1	19	20	19	15
Zr	2	127	142	135	177
Cr	20	110	100	90	170
Co	1	23	22	24	22
Ni	20	30	30	30	40
Cu	10	50	50	50	40
Zn	30	80	90	80	90
Ga	1	18	18	18	20
Ge	1	1	2	1	1
As	5	6	< 5	< 5	29
Rb	2	57	49	51	78
Nb	1	7	7	7	10
Mo	2	< 2	3	< 2	3
Ag	0.5	< 0.5	< 0.5	< 0.5	< 0.5
In	0.2	< 0.2	< 0.2	< 0.2	< 0.2
Sn	1	2	2	1	2
Sb	0.5	1	0.9	1	2
Cs	0.5	3.5	2.8	3	5.1
La	0.1	19.5	22.9	20.7	29
Ce	0.1	40.3	46.8	43.1	60
Pr	0.05	4.74	5.71	5.2	7.04
Nd	0.1	19.2	22.7	20.5	26.5

Table3
Click here to download Table: Table 3.xlsx

Table 3 – Chemical and isotopic compositions of noble gases from fumaroles.

Region	Locality	Lat.	Long.	Sample type	R/Ra	$^{4}He/^{20}Ne$	^{4}He ppm	^{20}Ne ppm	Rc/Ra	Error +/-
Central Volcanic Zone	Lastarria CCVG3 lower fumarolic field	-25.154166	-68.523888	Dry gas samples fumaroles	5.34	176.76	10.80	0.06	5.35	0.048
Central Volcanic Zone	Lastarria CCVG2 lower fumarolic field	-25.154166	-68.523888	Dry gas samples fumaroles	5.27	157.37	9.61	0.06	5.28	0.050
Central Andes Volcanic Zone	Lastarria	-25.154166	-68.523888	Lower fumarole field		159.9			5.14	
Central Andes Volcanic Zone	Lastarria	-25.154166	-68.523888	Lower fumarole field		199.1			5.13	
Central Andes Volcanic Zone	Lastarria	-25.154166	-68.523888	Lower fumarole field		-			5.13	
AIR					1	0.318	5.24	16.48		

Table4

Click here to download Table: Table 4.xlsx

Table 4 – Chemical and isotopic compositions of noble gases from fluid inclusions.

Sample ID	Period of volcanism	Mineral	Weight	^{4}He	^{20}Ne	^{40}Ar	^{36}Ar	R/Ra	$^{4}He/^{20}Ne$	Rc/Ra	Error tot +/-	$^{40}Ar/^{36}Ar$	Error
			g	mol/g	mol/g	mol/g	mol/g						%

APPENDIX1

Click here to download Background dataset for online publication only: APPENDIX I.xlsx

APPENDIX2

Click here to download Background dataset for online publication only: APPENDIX_II.xlsx

APPENDIX3

APPENDIX4

Click here to download Background dataset for online publication only: APPENDIX_IV.xlsx

APPENDIX5

Click here to download Background dataset for online publication only: APPENDIX_V.xlsx

APPENDIX6

Click here to download Background dataset for online publication only: APPENDIX_VI.xlsx

APPENDIX7

Click here to download Background dataset for online publication only: APPENDIX_VII.xlsx

APPENDIX8

Click here to download Background dataset for online publication only: APPENDIX_VIII.xlsx

APPENDIX9

APPENDIX10

*Declaration of Interest Statement

Declaration of interests

X The authors declare that they have no known competing financial interests or personal relationships that could have appeared to influence the work reported in this paper.

☐The authors declare the following financial interests/personal relationships which may be considered as potential competing interests: